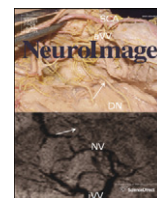




Contents lists available at SciVerse ScienceDirect

NeuroImage

journal homepage: www.elsevier.com/locate/ynimg

Interpretable whole-brain prediction analysis with GraphNet

Logan Grosenick^{a,b,*}, Brad Klingenberg^b, Kiefer Katovich^c, Brian Knutson^c, Jonathan E. Taylor^b^a Center for Mind, Brain, and Computation, Stanford University, Stanford, CA, USA^b Department of Statistics, Stanford University, Stanford, CA, USA^c Department of Psychology, Stanford University, Stanford, CA, USA

ARTICLE INFO

Article history:

Accepted 26 December 2012

Available online 5 January 2013

ABSTRACT

Multivariate machine learning methods are increasingly used to analyze neuroimaging data, often replacing more traditional “mass univariate” techniques that fit data one voxel at a time. In the functional magnetic resonance imaging (fMRI) literature, this has led to broad application of “off-the-shelf” classification and regression methods. These generic approaches allow investigators to use ready-made algorithms to accurately decode perceptual, cognitive, or behavioral states from distributed patterns of neural activity. However, when applied to correlated whole-brain fMRI data these methods suffer from coefficient instability, are sensitive to outliers, and yield dense solutions that are hard to interpret without arbitrary thresholding. Here, we develop variants of the Graph-constrained Elastic-Net (GraphNet), a fast, whole-brain regression and classification method developed for spatially and temporally correlated data that automatically yields interpretable coefficient maps (Grosenick et al., 2009b). GraphNet methods yield sparse but structured solutions by combining structured graph constraints (based on knowledge about coefficient smoothness or connectivity) with a global sparsity-inducing prior that automatically selects important variables. Because GraphNet methods can efficiently fit regression or classification models to whole-brain, multiple time-point data sets and enhance classification accuracy relative to volume-of-interest (VOI) approaches, they eliminate the need for inherently biased VOI analyses and allow whole-brain fitting without the multiple comparison problems that plague mass univariate and roaming VOI (“searchlight”) methods. As fMRI data are unlikely to be normally distributed, we (1) extend GraphNet to include robust loss functions that confer insensitivity to outliers, (2) equip them with “adaptive” penalties that asymptotically guarantee correct variable selection, and (3) develop a novel sparse structured Support Vector GraphNet classifier (SVGN). When applied to previously published data (Knutson et al., 2007), these efficient whole-brain methods significantly improved classification accuracy over previously reported VOI-based analyses on the same data (Grosenick et al., 2008; Knutson et al., 2007) while discovering task-related regions not documented in the original VOI approach. Critically, GraphNet estimates fit to the Knutson et al. (2007) data generalize well to out-of-sample data collected more than three years later on the same task but with different subjects and stimuli (Karmarkar et al., submitted for publication). By enabling robust and efficient selection of important voxels from whole-brain data taken over multiple time points (> 100,000 “features”), these methods enable data-driven selection of brain areas that accurately predict single-trial behavior within and across individuals.

© 2013 Elsevier Inc. Open access under CC BY-NC-ND license.

Introduction

Accurately predicting subject behavior from functional brain data is a central goal of neuroimaging research. In functional magnetic resonance imaging (fMRI) studies, investigators measure the blood oxygen-level dependent (BOLD) signal—a proxy for neural activity—and relate this signal to psychophysical or psychological variables of interest. Historically, modeling is performed one voxel at a time to yield a map of univariate statistics that are then thresholded according to some heuristic to yield a “brain map” suitable for visual

inspection. Over the past decade, however, a growing number of neuroimaging studies have applied machine learning analyses to fMRI data to model effects across multiple voxels. Commonly referred to as “multivariate pattern analysis” (Hanke et al., 2009) or “decoding” (to distinguish them from more commonly-used “mass-univariate” methods (Friston et al., 1995)), these approaches have allowed investigators to use activity patterns across multiple voxels to classify image categories during visual presentation (Peelen et al., 2009; Shinkareva et al., 2008), image categories during memory retrieval (Polyn et al., 2005), intentions to move (Haynes et al., 2007), and even intentions to purchase (Grosenick et al., 2008) (to name just a few applications—see also (Bray et al., 2009; Haynes and Rees, 2006; Norman et al., 2006; O’Toole et al., 2007; Pereira et al., 2009), and examples in *NeuroImage* Volume 56 Issue 2). In multiple cases,

* Corresponding author at: 220 Panama Street, Ventura Hall Rm. 30, Stanford, CA 94305.
Fax: +1 650 283 0010.

E-mail address: logang@gmail.com (L. Grosenick).

these statistical learning algorithms have shown better predictive performance than standard mass-univariate analyses (Haynes and Rees, 2006; Pereira et al., 2009).

Despite these advances, analysis of neuroimaging data with statistical learning algorithms is still young. Most of the research that has applied statistical learning algorithms to fMRI data has been conducted by a few laboratories (Norman et al., 2006), and most analyses have been conducted with off-the-shelf classifiers (Norman et al., 2006; Pereira et al., 2009, but cf. Brodersen et al., 2011; Chappell et al., 2009; Grosenick et al., 2008; Hutchinson et al., 2009; Michel et al., 2011; Ng et al., 2012). These classifiers are often applied to volume of interest (VOI) data within subjects rather than whole-brain data across subjects (Etzel et al., 2009; Pereira et al., 2009, but cf. Grosenick et al., 2009b; Michel et al., 2011; Mitchell et al., 2004; Mourão-Miranda et al., 2007; Ng et al., 2012; Ryali et al., 2010; van Gerven and Heskes, 2012). While these classifiers have a venerable history in the machine learning literature, they were not originally developed for application to whole-brain neuroimaging data, and so suffer from inefficiencies in this context. Specifically, the large number of features (usually voxel data) and spatiotemporal correlations characteristic of fMRI data present unique challenges for off-the-shelf classifiers.

Indeed, the purpose of off-the-shelf classifiers in the machine learning literature (e.g., discriminant analysis (DA), naive Bayes (NB), k-nearest neighbors (kNN), random forests (RF), and support vector machines (SVM)) has been to quickly and easily yield good classification accuracy—for example in speech recognition or

hand-written digit identification (Hastie et al., 2009). Beyond accuracy, however, neuroscientists often aim to understand which neural features are related to particular stimuli or behaviors at specific points in time. This distinct aim of interpretability requires classification or regression methods that can yield clearly interpretable sets of model coefficients. For this reason, the recent literature on classification of fMRI data has recommended using linear classifiers (e.g., logistic regression (LR), linear discriminant analysis (LDA), Gaussian Naive Bayes (GNB), or linear SVM) rather than nonlinear classifiers (Haynes and Rees, 2006; Pereira et al., 2009).

Linearity alone, however, does not guarantee that a method will yield a stable and interpretable solution. For instance, in the case of multiple correlated input variables LR, LDA, and GNB yield unstable coefficients and degenerate covariance estimates, particularly when applied to smoothed data (Hastie et al., 1995, 2009). In the context of classification, penalized least squares may over smooth coefficients, complicating interpretation (Friedman, 1997). Additionally, most linear classifiers return dense sets of coefficients (as in Fig. 1, left panels) that require subsequent thresholding or feature selection to yield parsimonious solutions. Although heuristic methods exist for coefficient selection, these are generally greedy (e.g., forward/backward stage-wise procedures like Recursive Feature Elimination (Bray et al., 2009; De Martino et al., 2007; Guyon et al., 2002)), yielding unstable solutions when data are resampled (since these algorithms tend to converge to local minima) (Hastie et al., 2009). Although principled methods exist for applying thresholds to dense mass-univariate coefficient maps (e.g. Random Field Theory (Adler and Taylor, 2000;

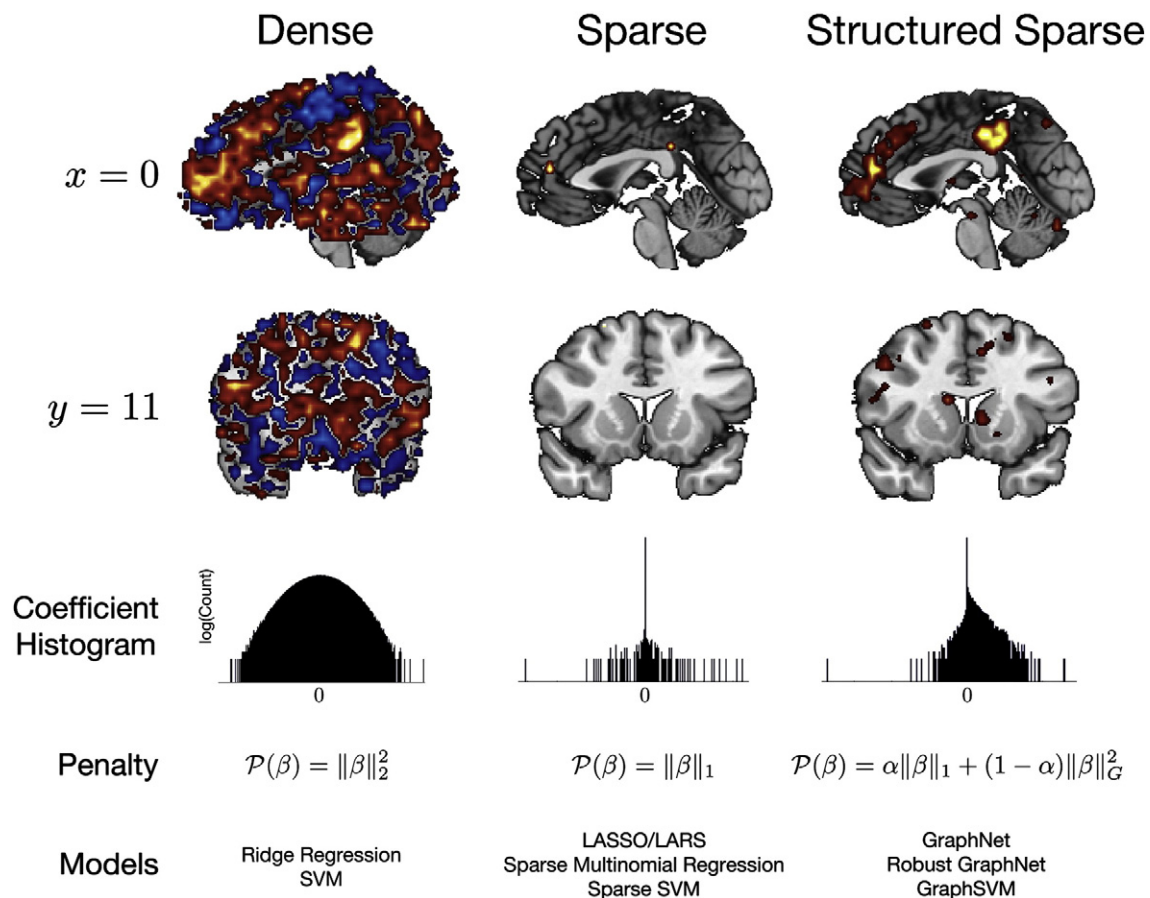


Fig. 1. Mid-sagittal and coronal plots of example coefficients from dense, sparse, and structured sparse coefficients (in Talairach coordinates). Warm colored coefficients indicate a positive relationship with the target variable (here predicting the decision to buy a product), cool colors a negative relationship. Sparse methods set many coefficients to zero, while in dense methods almost all coefficients are nonzero. Structured sparse methods use a penalty on differences between selected voxels to impose a structure on the fit so that it yields coefficients that are both sparse and structured (e.g., smooth). Log-histograms of the estimated voxel-wise coefficients show that the sparse method coefficients have a near-Laplacian (double-exponential) distribution, while the dense coefficients have a near-Gaussian distribution. The structured sparse coefficients are a product of these distributions (see also Fig. 2). Coefficient penalties that yield each result and examples of related methods are given below each column.

Worsley et al., 2004)), these approaches do not currently extend to dense multivariate regression or classification methods.

Recently, sparse regression methods have been applied to neuroimaging data to yield reduced coefficient sets that are automatically selected during model fitting. The first examples in the fMRI literature include Yamashita et al. (2008), who applied sparse logistic regression (Tibshirani, 1996) to classification of visual stimuli, and Grotenick et al. (2008) who first developed sparse penalized discriminant analysis by converting an “Elastic-Net” regression (Zou and Hastie, 2005) into a classifier, and then applied it to choice prediction. Subsequently, sparse methods for regression (Carroll et al., 2009; Hanke et al., 2009) and classification (Hanke et al., 2009) have been applied to fMRI data to yield reduced sets of coefficients from volumes of interest, whole-brain volumes (Ryali et al., 2010; van Gerven et al., 2010), and whole-brain volumes over multiple time points (Grotenick et al., 2009b). These methods typically impose an ℓ_1 -penalty (sum of absolute values) on the model coefficients, which sets many of the estimated coefficients to zero (see Fig. 1, leftmost panels, and Fig. 2b). When applied to correlated fMRI data, however, ℓ_1 -penalized methods can select an overly sparse solution—resulting in omission of relevant features as well as unstable coefficient estimates during cross-validation (Grotenick et al., 2008; Zou and Hastie, 2005). To allow relevant but correlated coefficients to coexist in a sparse model fit, recent approaches to fMRI regression (Carroll et al., 2009; Li et al., 2009) and classification (Grotenick et al., 2008, 2009b; Ryali et al., 2010) impose a hybrid of both ℓ_1 - and ℓ_2 -norm penalties (the “Elastic-Net” penalty of Zou and Hastie (2005)) on the coefficients. These hybrid approaches allow the inclusion of correlated variables in sparse model fits.

This paper explores modified methods that combine the Elastic-Net penalty with a general user-specified sparse graph penalty. This sparse graph penalty allows the user to efficiently incorporate physiological constraints and prior information (such as smoothness in space or time or anatomical details such as topology or connectivity) in the model. The resulting Graph-constrained Elastic-Net (or “GraphNet”) regression (Grotenick et al., 2009b) has the capacity to find “structured sparsity” in correlated data with many features (Fig. 1, right panels), consistent with previous results in the manifold learning (Belkin et al., 2006) and gene microarray literatures (Li and Li, 2008). In the statistics literature, related “sparse structured” methods have been shown to have desirable convergence and variable selection properties for large correlated data sets (Jenatton et al., 2011; Slawski et al., 2010). These

sparse, structured models can also be implemented within a Bayesian framework (van Gerven et al., 2010). Here, we extend the performance of GraphNet regression and classification methods to whole-brain fMRI data by: (1) generalizing them to be robust to outliers in fMRI data (for both regression and classification), (2) adding “adaptive” penalization to reduce fit bias and improve variable selection, and (3) developing a novel support vector GraphNet (SVGN) classifier. Additionally, to efficiently fit GraphNet methods to whole-brain fMRI data over multiple time-points, we adapt algorithms from the applied statistics literature (Friedman et al., 2010).

After developing robust and adaptive GraphNet regression and classification methods, we demonstrate the enhanced performance of GraphNet classifiers on previously published data (Karmarkar et al., submitted for publication; Knutson et al., 2007). Specifically, we use GraphNet methods to predict subjects’ trial-to-trial purchasing behavior with whole-brain data over several time points, and then infer which brain regions best predict upcoming choices to purchase or not purchase a product. Fitting these methods to 25 subjects’ whole-brain data over 7 time points (2 s TRs) yielded classification rates which exceeded those found previously in a volume of interest (VOI) based classification analysis (Grotenick et al., 2008), as well as those obtained with a linear support vector machine (SVM) classifier fit to the whole brain data. While the GraphNet results on whole-brain data confirm the relevance of previously chosen volumes of interest (i.e., bilateral nucleus accumbens (NAcc), medial prefrontal cortex (MPFC), and anterior insula), they also implicate previously unchosen areas (i.e., ventral tegmental area (VTA) and posterior cingulate). We conclude with a discussion of the interpretation of GraphNet model coefficients, as well as future improvements, applications, and extensions of this family of GraphNet methods to neuroimaging data. Open source code for solving the GraphNet problems in this paper is freely available at <https://github.com/logang/neuroparser>.

Methods

Background

Penalized least squares

Many classification and regression problems can be formulated as modeling a response vector $y \in \mathbb{R}^n$ as a function of data matrix $X \in \mathbb{R}^{n \times p}$, which consists of n observations each of length p (with $n \geq p$).

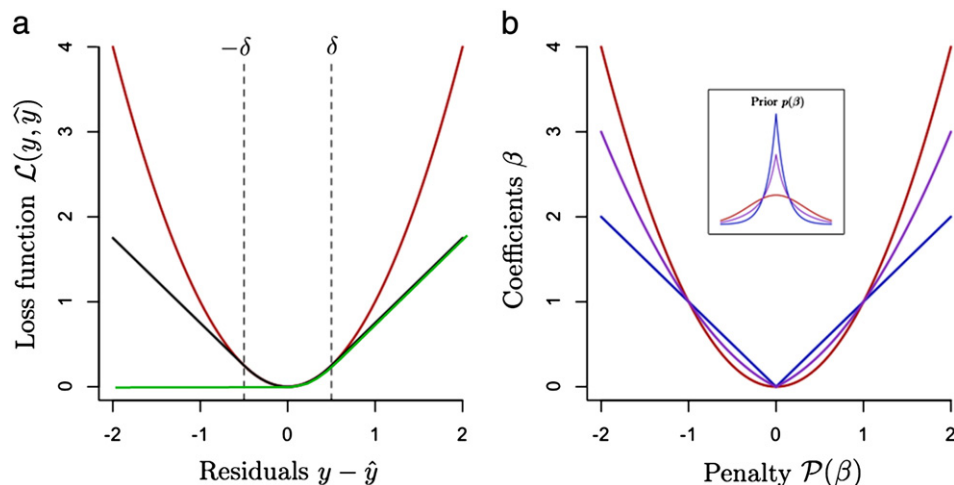


Fig. 2. (a) Diagrammatic representation of squared-error (red), Huber (black), and Huberized Hinge (green) loss functions. Dotted lines denote where the Huber loss changes from penalizing residuals quadratically (where $|y - \hat{y}| \leq \delta$) to penalizing them linearly (where $|y - \hat{y}| > \delta$). The linear penalty on large residuals makes the Huber loss robust. (b) Diagrammatic representation of convex penalty functions used in this article (along one coordinate β). The red curve is a quadratic penalty $\mathcal{P}(\beta) = \beta^2$ on coefficient magnitude, often called the Tikhonov or “ridge” penalty in regression. The blue curve is the lasso penalty on coefficient magnitude $\mathcal{P}(\beta) = |\beta|$. The purple curve is a convex combination of the red and blue curves: $\mathcal{P}(\beta) = \alpha\beta^2 + (1-\alpha)|\beta|$ (where here $\alpha = 0.5$, called the “Elastic-Net” penalty). The inset shows the shape of the prior distribution on the coefficient estimates that each of these penalties corresponds to: Gaussian (red), Laplacian (blue), and mixed Gaussian and Laplacian (purple) (units arbitrary). The priors become increasingly peaked around zero as the Elastic-Net penalty approaches the Lasso penalty, corresponding to a prior belief that many coefficients will be exactly zero.

In particular, a large number of models treat y as a linear combination of the predictors in the presence of noise $\epsilon \in \mathbb{R}^n$, such that

$$y = X\beta + \epsilon, \quad (1)$$

where ϵ is a noise vector typically assumed to be normally distributed $\epsilon \sim \mathcal{N}(0, I\sigma^2)$ with vector mean 0 and diagonal variance–covariance matrix $I\sigma^2$ and $\beta \in \mathbb{R}^p$ a vector of linear model coefficients. In this case using squared error loss leads to the well-known ordinary least squares (OLS) solution

$$\hat{\beta} = \underset{\beta}{\operatorname{argmin}} \|y - X\beta\|_2^2 = (X^T X)^{-1} X^T y, \quad (2)$$

which yields the best linear unbiased estimator (BLUE) if the columns of X are uncorrelated (Lehmann and Casella, 1998).

However, this estimator is inefficient in general for $p > 2$ —it is dominated by biased estimators (Stein, 1956)—and if the columns of X are correlated (i.e. are “multicollinear”) then the estimated coefficient values can vary erratically with small changes in the data, so the OLS fit can be quite poor. A common solution to this problem is penalized (or “regularized”) least squares regression (Tikhonov, 1943), in which the magnitudes of the model coefficients are penalized to stabilize them. This is accomplished by adding a penalty term $\mathcal{P}(\beta)$ on the coefficient vector β , yielding

$$\hat{\beta} = \underset{\beta}{\operatorname{argmin}} \|y - X\beta\|_2^2 + \lambda \mathcal{P}(\beta), \lambda \in \mathbb{R}_+, \quad (3)$$

where λ is a parameter that trades off least squares goodness-of-fit with the penalty on the model coefficients (or equivalently, trades off fit variance for fit bias) and \mathbb{R}_+ is the set of nonnegative scalars. These estimates are equivalent to maximum a posteriori (MAP) estimates from a Bayesian perspective (with a Gaussian prior on the coefficients if $\mathcal{P}(\beta) = \|\beta\|_2^2$ (Hastie et al., 2009)), or to the Lagrangian relaxation of a constrained bi-criterion optimization problem (Boyd and Vandenberghe, 2004). Such equivalencies motivate various interpretations of the model coefficients and parameter λ (see the section “Interpreting GraphNet regression and classification”).

Sparse regression and automatic variable selection

There are a few standard choices for the penalty $\mathcal{P}(\beta)$. Letting $\mathcal{P}(\beta) = \|\beta\|_2^2 = \sum_{j=1}^p \beta_j^2$ (the ℓ_2 norm) gives the classical Tikhonov or “ridge” regression estimates originally proposed for such problems (Hoerl and Kennard, 1970; Tikhonov, 1943). More recently, the choice $\mathcal{P}(\beta) = \|\beta\|_1 = \sum_{j=1}^p |\beta_j|$ (the ℓ_1 norm)—called the Least Absolute Shrinkage and Selection Operator (or “lasso”) penalty in the regression context (Tibshirani, 1996)—has become widely popular in statistics, engineering, and computer science, leading some to call such ℓ_1 -regression the “modern least squares” (Candes et al., 2008). In addition to shrinking the coefficient estimates, the lasso performs variable selection by producing sparse coefficient estimates (i.e., many are exactly equal to zero, see Fig. 1 left panels). In many applications, having a sparse vector $\hat{\beta}$ is highly desirable, since a fit with fewer non-zero coefficients is simpler, and can help select predictors that have an important relationship with the response variable y .

The ℓ_1 -norm used in the lasso is the closest convex relaxation of the ℓ_0 pseudo-norm $\|\beta\|_0 = \sum_{j=1}^p 1_{\{\beta_j \neq 0\}}$, where $1_{\{\beta_j \neq 0\}}$ is an indicator function that is 1 if the j th coefficient β_j is nonzero and 0 otherwise. This represents a penalty on the number of nonzero coefficients (their cardinality). However, finding a minimal cardinality solution generally involves a combinatorial search through possible sets of nonzero coefficients (a form of “all subsets regression” (Hastie et al., 2009)) and so is computationally infeasible for even a modest number of input features. An ℓ_1 -norm penalty can be used as a heuristic that results in coefficient sparsity (which corresponds to the maximum a posteriori (MAP) estimates under a Laplacian (double-exponential) prior; for a fully Bayesian

approach see van Gerven et al. (2010)). Such ℓ_1 -penalized regression methods set many variables equal to zero and automatically select only a small subset of relevant variables to assign nonzero coefficients. While these methods yield the sparsest possible fit in many cases (Candes et al., 2003; Donoho, 2006), they do not always do so, and reweighted methods (e.g., Automatic Relevance Determination (ARD) (Wipf and Nagarajan, 2008) and iterative reweighting of the ℓ_1 penalty (Candes et al., 2008)) exist for finding sparser solutions. It is worth noting that while Bayesian methods for variable selection (such as Relevance Vector Machines) have existed in the literature for some time, these methods typically require using EM-like or MCMC approaches that do not guarantee convergence to a global minimum and that are relatively computationally inefficient (though see Mohamed et al. (2011) for an interesting counter-point). As an interesting exception, recent work on ARD and sparse Bayesian learning (Wipf and Nagarajan, 2008) has provided an attractive alternative, showing that the sparse Bayesian learning problem can be solved as a sequence of reweighted lasso problems, similar to the adaptive methods discussed below. This approach no longer provides a full posterior, but does provide an interesting and computationally tractable link to the Bayesian formulation. In the future we expect that such links will lead to better approaches for model selection in these methods than the “brute force” grid search employed here.

Elastic-Net regression

Despite offering a sparse solution and automatic variable selection, there are several disadvantages to using ℓ_1 -penalized methods like the lasso in practice. For example, from a group of highly correlated predictors, the lasso will typically select a subset of “representative” predictors to include in the model fit (Zou and Hastie, 2005). This can make it difficult to interpret coefficients because those that are set to 0 may still be useful for modeling y (i.e., false negatives are likely). Worse, entirely different subsets of coefficients may be selected when the data are resampled (e.g., during cross-validation). Moreover, the lasso can select at most n non-zero coefficients (Zou and Hastie, 2005), which may prove undesirable when the number of input features (p) exceeds the number of observations (n) (i.e., “ $p \gg n$ ” problems). Finally, as a global shrinkage method, the lasso biases model coefficients towards zero (Hastie et al., 2009; Tibshirani, 1996), making interpretation with respect to original data units difficult. Other methods that use only an ℓ_1 penalty (e.g., sparse logistic/multinomial regression and sparse SVM (Hastie et al., 2009)) are subject to the same deficiencies.

In response to several of these concerns Zou and Hastie (2005) proposed the Elastic-Net, which uses a mixture of ℓ_1 - and ℓ_2 -norm regularization, and may be written

$$\hat{\beta} = \kappa \underset{\beta}{\operatorname{argmin}} \|y - X\beta\|_2^2 + \lambda_1 \|\beta\|_1 + \lambda_2 \|\beta\|_2^2, \quad (4)$$

where the factor $\kappa = 1 + \lambda_2$ in (4) and subsequent equations is a rescaling factor discussed in further detail below. This Elastic-Net estimator overcomes several (though not all) of the disadvantages discussed above, while maintaining many advantages of Tikhonov (“ridge”) regression and the lasso. In particular, the Elastic-Net accommodates groups of correlated variables and can select up to p variables with non-zero coefficients. The amount of sparsity in the solution vector can be tuned by adjusting the penalty coefficients λ_1 and λ_2 . In this case, the ℓ_1 penalty can be thought of as a heuristic for enforcing sparsity, while the ℓ_2 penalty allows correlated variables to enter the model and stabilizes the sample covariance estimate. This Elastic-Net approach performs well on fMRI data in both regression and classification settings (Carroll et al., 2009; Groseknick et al., 2008; Ryali et al., 2010).

Graph-constrained Elastic-Net (GraphNet) regression

So far we have seen that sparse regression methods like the Elastic-Net, which use a hybrid ℓ_1 - and ℓ_2 -norm penalty, can be used

to yield sparse model fits that do not exclude correlated variables (Zou and Hastie, 2005), and that we can turn these regression methods into classifiers that perform well when fit to VOI data (Grosenick et al., 2008). However, the Elastic-Net penalty merely makes the model fitting procedure “blind” to correlations between input features (by shrinking the sample estimate of the covariance matrix towards the identity matrix). Indeed, if λ_2 in Eq. (9) grows large, this method is equivalent to applying a threshold to mass-univariate OLS regression coefficients (i.e., the estimate of the covariance matrix becomes a scaled identity matrix) (Zou and Hastie, 2005).

In this section, we describe a modification of the Elastic-Net that explicitly imposes structure on the model coefficients. This allows the analyst to pre-specify constraints on the model coefficients (e.g., based on prior information like local smoothness, connectivity, or other desirable fit properties), and then to tune how strongly the fit adheres to these constraints. Since the user-specified constraints take the general form of an undirected graph, we call this regression method the Graph-constrained Elastic-Net (or “GraphNet”) (Grosenick et al., 2009b).

GraphNet closely resembles the Elastic-Net, but with a modification to the ℓ_2 -norm penalty term:

$$\hat{\beta} = \kappa \operatorname{argmin}_{\beta} \|y - X\beta\|_2^2 + \lambda_1 \|\beta\|_1 + \lambda_G \|\beta\|_G^2 \quad (5)$$

$$\|\beta\|_G^2 = \beta^T G \beta = \sum_{j=1}^p \sum_{k=1}^p \beta_j G_{jk} \beta_k,$$

where G is a sparse graph. Note that in the case where $G = I$, where I denotes the identity matrix, the GraphNet reduces back to the Elastic-Net. Thus the Elastic-Net is a special case of GraphNet and we can replicate the effects of increasing an Elastic-Net penalty by adding a scaled version of the identity matrix ($\lambda_2/\lambda_G I$ to G (for $\lambda_G > 0$)).

The example we will use for the matrix G in the remainder of this paper is the graph Laplacian, which formalized our intuition that voxels that are neighbors in time and space should typically have similar values. If we take the coefficients β to be functions over the brain volume $V \in \mathbb{R}^3$ over time points $T \in \mathbb{R}$ such that $\beta(x, y, z, t)$, then we would like a penalty that penalizes roughness in the coefficients as measured by their derivatives over space and time, such as

$$\mathcal{P}(\beta) = \int_{V,T} \left(\frac{\partial^2 \beta}{\partial x^2} + \frac{\partial^2 \beta}{\partial y^2} + \frac{\partial^2 \beta}{\partial z^2} + \frac{\partial^2 \beta}{\partial t^2} \right) dx dy dz dt$$

$$= \int_{V,T} \Delta \beta dx dy dz dt, \quad (6)$$

where Δ is the Laplacian operator, which here is a 4D isotropic measure of the second spatio-temporal derivative of the volumetric time-series. Since we are sampling discretely, we use the discrete approximation to the Laplacian operator Δ : the matrix Laplacian $L = D - A$ (the difference between the degree matrix D and the adjacency matrix A , see e.g., (Hastie et al., 1995)). This formulation generalizes well to arbitrary graph connectivity and is widely used in spectral clustering techniques and spectral graph theory (Belkin and Niyogi, 2008).

In the case where $G = L$, the graph penalty, $\|\beta\|_G^2$, has the appealingly simple representation

$$\|\beta\|_G^2 = \sum_{(i,j) \in \mathcal{E}_G} (\beta_i - \beta_j)^2,$$

where \mathcal{E}_G is the set of index pairs for voxels that share an edge in graph G (i.e. have a nonzero entry in the adjacency matrix A). Written this way, the graph penalty induces smoothness by penalizing the size of the pairwise differences between coefficients that are adjacent in the graph. In the one dimensional case, if the quadratic terms $(\beta_i - \beta_j)^2$ were replaced by absolute deviations $|\beta_i - \beta_j|$ then this would instead be an instance of the “fused lasso” (Tibshirani et al., 2005) or

generalized lasso (Tibshirani and Taylor, 2011). There are two main reasons for preferring a quadratic penalty in the present application:

1. The fused lasso is closely related to Total Variation (TV) denoising (Rudin et al., 1992) and tends to set many of the pairwise differences $\beta_i - \beta_j$ to zero, creating a sharp piecewise constant set of coefficients that lacks the spatial smoothness often expected in fMRI data. Extending this formulation to processes with more than one spatial or temporal dimension is nontrivial (Michel et al., 2011).
2. Significant algorithmic complications can be avoided by choosing a differentiable penalty on the pairwise differences (Friedman et al., 2007a; Tseng, 2001), speeding up model fitting and reducing model complexity considerably—especially in the case of spatial data, where the Total Variation penalty must be formulated as a more complicated sum of non-smooth norms on each of the first-order forward finite difference matrices (Michel et al., 2011; Wang et al., 2008b).

Thus GraphNet methods provide a sparse and structured solution similar to the fused lasso, generalized lasso, and Total Variation. However, unlike these approaches, GraphNet methods allow for smooth rather than piecewise constant structure in the non-sparse parts of the reconstructed volume. This is of interest in cases where we might expect the magnitudes of nonzero coefficients to be different within a volume of interest. Due to the smoothness of the graph penalty GraphNet methods are also easier from an optimization perspective. Of course, there are certainly situations in which the piecewise smoothness of Total Variation could be a better prior (this depends on the data and problem formulation).

Adaptive GraphNet regression

The methods described above automatically select variables by shrinking coefficient estimates towards zero, resulting in downwardly biased coefficient magnitudes. This shrinkage makes it difficult to interpret coefficient magnitude in terms of original data units, and severely restricts the conditions under which the lasso can perform consistent variable selection (Zou, 2006). Ideally, given infinite data, the method would select the correct parsimonious set of features (i.e., the “true model”, were it known), but avoid shrinking nonzero coefficients that remain in the model (unbiased estimation). Together, these desiderata are known as the “oracle” property (Fan and Li, 2001). Note that in the neuroimaging context, the first (consistent variable selection) corresponds to correct localization of signal, while the second (consistent coefficient estimation) relates to improving estimates of coefficient magnitude.

Several estimators possessing the oracle property (given certain conditions on the data) have been reported in the literature, including the adaptive lasso (Zhou et al., 2011; Zou, 2006) and the adaptive Elastic-Net (Zou and Zhang, 2009). These estimators are straightforward modifications of penalized linear models. They work by starting with some initial estimates of the coefficients obtained by fitting the non-adaptive model (Zou and Zhang, 2009), and use these to adaptively reweight the penalty on each individual coefficient β_j , $j = 1, \dots, p$. Recently Slawski et al., (2010) extended the adaptive approach to a sparse, structured method equivalent to GraphNet regression, and proved that the oracle properties previously shown for the adaptive lasso and adaptive Elastic-Net extend to the sparse, structured case provided the true coefficients are in the null space of G (i.e. the nonzero entries of β specify a connected component in G). We refer the reader to Slawski et al., (2010) for further details.

As in Slawski et al., (2010), we may rewrite the GraphNet to have an adaptive penalty (the adaptive GraphNet) as follows:

$$\hat{\beta} = \operatorname{argmin}_{\beta} \|y - X\beta\|_2^2 + \lambda_1^* \sum_{j=1}^p \hat{w}_j |\beta_j| + \lambda_G \|\beta\|_G^2 \quad (7)$$

$$\hat{w}_j = |\tilde{\beta}_j|^{-\gamma}. \quad (8)$$

The idea here is that important coefficients will have large starting estimates $\tilde{\beta}_j$ (where $\tilde{\beta}_j$ is a suitable estimator of β_j) and so will be shrunk at a rate inversely proportional to their starting estimates, leaving them asymptotically unbiased. On the other hand, coefficients with small starting estimates $\tilde{\beta}_j$ will experience additional shrinkage, making them more likely to be excluded. We let $\gamma = 1$ as in the finite sample case (Zou, 2006; Zou and Zhang, 2009), and by analogy to the adaptive Elastic-Net (Zou and Zhang, 2009) set $\tilde{\beta}$ to the standard GraphNet coefficient estimates for a fixed value of λ_G (chosen based on the GraphNet performance at that value). We use λ_1^* to differentiate the adaptive fit sparsity parameter from the parameter associated with the GraphNet fit used to initialize the weights \hat{w}_j .

It is important to note that the oracle properties that hold in the asymptotic case may not apply to the finite sample, $p \gg n$ situation. Nevertheless, we include these methods for comparison since oracle properties are desirable and since evidence suggests that the adaptive Elastic-Net has improved finite sample performance because it deals well with collinearity (Zou and Zhang, 2009).

Turning sparse regression methods into classifiers: Optimal Scoring (OS) and Sparse Penalized Discriminant Analysis (SPDA)

Sparse regression methods like the lasso or Elastic-Net can be turned into sparse classifiers (Clemmensen et al., 2011; Groseknick et al., 2008; Leng, 2008). Naively, we might imagine performing a two-class classification simply by running a regression with lasso or the Elastic-Net on a target vector containing 1's and 0's depending on the class of each observation $y_i \in \{0,1\}$. We would then take the predicted values from the regression \hat{y} and classify to 0 if the i th estimate $\hat{y}_i < 0.5$ and to 1 if the estimate $\hat{y}_i > 0.5$ (for example). In the multi-class case (i.e. J classes with $J > 2$), multi-response linear regression could be used as a classifier in a similar way. This would be done by constructing an indicator response matrix Y , with n rows and J columns (where again n is the number of observations and J is the number of classes). Then the i th row of Y has a 1 in the j th column if the observation is in the j th class and a 0 otherwise. If we run a multiple linear regression of Y on predictors X , we can classify by assigning the i th observation to the class having the largest fitted value $\hat{Y}_{i1}, \hat{Y}_{i2}, \dots, \hat{Y}_{iJ}$. With the exception of binary classification on balanced data, this classifier has several disadvantages. For instance, the estimates \hat{Y}_{ij} are not probabilities, and in the multi-class case certain classes can be “masked” by others, resulting in decreased classification accuracy (Hastie et al., 2009). However, applying LDA to the fitted values of such a multiple linear regression classifier is mathematically equivalent to fitting the full LDA model (Breiman and Ihaika, 1984), yielding posterior probabilities for the classes and dramatically improving classifier performance over the original multivariate regression in some cases (Hastie et al., 1994, 1995, 2009).

Hastie et al. (1994) and Hastie et al. (1995) exploit equivalences between multiple regression and LDA and between LDA and canonical correlation analysis to develop a procedure they call Optimal Scoring (OS). OS allows us to build a classifier by first fitting a multiple regression to Y using an arbitrary regression method, and then linearly transforming the fitted results of this regression using the OS procedure (see Hastie et al. (1994) for further algorithmic and statistical details). This procedure yields both class probability estimates and discriminant coordinates, and allows us to use any number of regression methods as discriminant classifiers. This approach is discussed in detail for nonlinear regression methods applied to a few input features in Hastie et al. (1994), and for regularized regression methods applied to numerous (i.e., hundreds of) correlated input features in Hastie et al. (1995). Here we extend the results of the latter work to include sparse structured regression methods that can be fit efficiently to hundreds of thousands of input features.

More formally, OS finds an optimal scoring function $\theta: g \rightarrow \mathbb{R}$ that maps classes $g \in \{1, \dots, J\}$ into the real numbers. In the case of a multi-class classification using the Elastic-Net, we can apply OS to yield estimates

$$(\hat{\theta}, \hat{\beta}) = \kappa \operatorname{argmin}_{\theta, \beta} \|Y\theta - X\beta\|_2^2 + \lambda_1 \|\beta\|_1 + \lambda_2 \|\beta\|_2^2 \quad (9)$$

$$\text{subject to } n^{-1} \|Y\theta\|_2^2 = 1, \quad (10)$$

where θ is a matrix that yields the optimal scores when applied to indicator matrix Y , and where we add the constraint (10) to avoid degenerate solutions (Groseknick et al., 2008). Given that this is just a sparse version of PDA (Hastie et al., 1995), we have called this combination Sparse Penalized Discriminant Analysis (SPDA). It has also recently been called Sparse Discriminant Analysis (SDA) Clemmensen et al. (2011) (and for an interesting alternative approach for constructing sparse linear discriminant classifiers, see Witten and Tibshirani (2011)).

The SPDA-GraphNet is defined as

$$(\hat{\theta}, \hat{\beta}) = \kappa \operatorname{argmin}_{\theta, \beta} \|Y\theta - X\beta\|_2^2 + \lambda_1 \|\beta\|_1 + \lambda_G \|\beta\|_G^2 \quad (11)$$

$$\text{subject to } n^{-1} \|Y\theta\|_2^2 = 1. \quad (12)$$

It is important to note that the direct equivalence between penalized OS and penalized LDA has only recently been proven in the binary classification case, and does not hold for multi-class classification problems (Merchante et al., 2012). However, both approximate methods that iteratively minimize over θ and β (Clemmensen et al., 2011) and equivalent methods based on the Group Lasso (Merchante et al., 2012) could be used with GraphNet regression methods to build multi-class GraphNet classifiers. We note that in the binary classification case there are at least two options to turn regression methods into classifiers: Optimal Scoring and logistic regression (see e.g. Friedman et al., 2010). In the case of multiple classes, the approaches of (Clemmensen et al., 2011; Merchante et al., 2012) provide LDA or LDA-like classifiers. Sparse multinomial regression could also be used in the multi-class case. Any of these approaches may be used to turn GraphNet regression methods into GraphNet classifiers. Because Optimal Scoring converts regression methods into equivalent linear discriminant classifiers, it allows us to combine notions from regression such as degrees of freedom with notions from discriminant analysis such as class visualization in the discriminant space using discriminant coordinates and trial-by-trial posterior probabilities for individual observations (Hastie et al., 1995). This, and its greater computational simplicity over logistic and multinomial regressions, make OS an appealing approach.

Turning regression methods into classifiers: relating Support Vector Machines (SVM) to penalized regression

In addition to the LDA and logistic/multinomial approaches to classification, maximum margin classifiers like SVM have been very successful. As we will also be developing a Support Vector GraphNet (SVGN) variant below, we briefly discuss how support vector machines can be related to regression methods like those described above. If the data are centered such that an intercept term can be ignored, the SVM solution can be written

$$\hat{\beta} = \operatorname{argmin}_{\beta} \sum_{i=1}^n (1 - y_i x_i^T \beta)_+ + (\lambda/2) \|\beta\|_2^2,$$

where $(\cdot)_+$ indicates taking the positive part of the quantity in parentheses. In this function estimation formulation of the SVM problem, we see the similarity to the penalized regression methods above:

the only difference is that the usual squared error loss $L(y_i, x_i, \beta) = (y_i - x_i^T \beta)^2$ has been replaced by the “hinge loss” function $L_H(y_i, x_i, \beta) = (1 - y_i x_i^T \beta)_+$. This function is non-differentiable, and more recent work (Wang et al., 2008a) uses a differentiable “Huberized hinge loss” (Fig. 2a), which we will discuss in greater detail below. The important point here is that formulating the SVM problem as a loss term and a penalty term reveals how we might build an SVM with more general penalization, such as that used in GraphNet regression methods above.

Novel extensions of GraphNet methods

Robust GraphNet and adaptive robust GraphNet

More generally, we can formulate the penalized regression problem of interest as minimizing the penalized empirical risk $\mathcal{R}_p(\beta)$ as a function of the coefficients, so that

$$\hat{\beta} = \underset{\beta}{\operatorname{argmin}} \mathcal{R}_p(\beta) = \underset{\beta}{\operatorname{argmin}} \mathcal{R}(y, \hat{y}) + \lambda \mathcal{P}(\beta), \quad (13)$$

where \hat{y} is the estimate of response variable y (note $\hat{y} = X \hat{\beta}$ in the linear models we consider) and $\mathcal{R}(y, \hat{y}) = n^{-1} \sum_{i=1}^n L(y_i, \hat{y}_i)$ is the average of the loss function over the training data (the “empirical risk”) of the loss function $L(y_i, \hat{y}_i)$ that penalizes differences between the estimated and true values of y at the i th observation. For example, in Eqs. (3)–(9) we used $\mathcal{R}(y, \hat{y}) = \|y - \hat{y}\|_2^2 = \sum_{i=1}^n (y_i - \hat{y}_i)^2$ (“squared error loss”). While squared error loss enjoys many desirable properties under the assumption of Gaussian noise, it is sensitive to the presence of outliers.

Outlying data points are an important consideration when modeling fMRI data, in which a variety of factors ranging from residual motion artifacts to field inhomogeneities can cause some observations to fall far from the sample mean. In the case of standard squared-error loss (as in Eqs. (2)–(9)), these outliers can have undue influence on the model fit due to the quadratically increasing penalty on the residuals (see Fig. 2a). A standard solution in such cases is to use a robust loss function, such as the Huber loss function (Huber and Ronchetti, 2009),

$$\mathcal{R}_H(y, \hat{y}; \delta) = n^{-1} \sum_{i=1}^n L_\delta(y_i - \hat{y}_i) \quad (14)$$

where

$$L_\delta(y_i - \hat{y}_i) = \begin{cases} (y_i - \hat{y}_i)^2 / 2 & \text{for } |y_i - \hat{y}_i| \leq \delta \\ \delta |y_i - \hat{y}_i| - \delta^2 / 2 & \text{for } |y_i - \hat{y}_i| > \delta \end{cases}$$

This function penalizes residuals quadratically when they are less than or equal to parameter δ , and linearly when they are larger than δ (Fig. 2a). A well specified δ can thus significantly reduce the effects of large residuals (outliers) on the model fit, as they no longer have the leverage resulting from a quadratic penalty. As $\delta \rightarrow \infty$ (or practically, when it becomes larger than the most outlying residual) we recover the standard squared-error loss.

Since GraphNet uses squared-error loss, it can now be modified to include a robust penalty like the Huber loss defined above. Replacing the squared error loss function with the loss function (Eq. (14)) yields

$$\hat{\beta} = \underset{\beta}{\operatorname{argmin}} \mathcal{R}_H(y, X\beta; \delta) + \lambda_1 \|\beta\|_1 + \lambda_G \|\beta\|_G^2. \quad (15)$$

The adaptive robust GraphNet is then a straightforward generalization (see the section “Adaptive GraphNet regression”, as well as the next section).

The SPDA-RGN classifier can be defined like the standard GraphNet classifier (Eq. (11)). However, the SPDA-RGN classifier now has an additional hyperparameter to be estimated (or assumed). Specifically,

the value of δ determines where the loss function switches from quadratic to linear (Fig. 2a). Further, the loss function on the residuals is no longer quadratic and therefore could slow down optimization convergence. We discuss a solution to this issue next.

Infimal convolution for non-quadratic loss functions

In order to solve both the robust GraphNet, adaptive robust GraphNet, and Support Vector GraphNet problems efficiently, we introduce a general method for solving coordinate-wise descent problems with smooth, non-quadratic convex loss functions as penalized least squares problems in an augmented set of variables.

Convergence speed of subgradient methods such as coordinate-wise descent can be substantially improved when the loss function takes a quadratic form, while non-quadratic loss functions can take numerous iterations to converge for each coefficient, significantly increasing computation time. However, we can circumvent these problems and extend the applicability of coordinate-wise descent methods using a trick from convex analysis to rewrite these loss functions as quadratic forms in an augmented set of variables. This method is called infimal convolution (Rockafellar, 1970), and is defined as

$$(f \star_{\text{inf}} g)(x) := \inf_y \{f(x - y) + g(y) | y \in \mathbb{R}^n\}, \quad (16)$$

where f and g are two functions of $x \in \mathbb{R}^p$. In this way it is possible to rewrite the i th term in the Huber loss function (Eq. (14)) as the infimal convolution of the squared and absolute-value functions applied to the i th residual r_i :

$$\rho_\delta(r_i) = \left((1/2)(\cdot)^2 \star_{\text{inf}} |\cdot| \right)(r_i) = \inf_{a_i + b_i = r_i} a_i^2 / 2 + \delta |b_i|, \quad (17)$$

where $r_i = y_i - (X\beta)_i$ (note that a dot (\cdot) is used to indicate the functional nature of the expression without having to add additional dummy variables). This yields the augmented estimation problem

$$(\hat{\alpha}, \hat{\beta}) = \underset{\alpha, \beta}{\operatorname{argmin}} (1/2) \|y - X\beta - \alpha\|_2^2 + \lambda_G \beta^T G \beta + \delta \|\alpha\|_1 + \lambda_1 \|\beta\|_1, \quad (18)$$

where we have introduced the auxiliary variables $\alpha \in \mathbb{R}^n$. Considering the residuals r_i , the first term in the objective of Eq. (18) can be written $(1/2) \|y - X\beta - \alpha\|_2^2 = (1/2) \sum_i (r_i - \alpha_i)^2$ and thus each α_i can directly reduce the residual sum of squares corresponding to a single observation by taking a value close to r_i . Since for some δ the penalty $\delta \|\alpha\|_1$ requires the α vector to be k -sparse, this formulation intuitively allows a linear rather than a quadratic penalty to be placed on k of the residuals (with k tuned by choice of δ as expressed in the Huber loss formulation). These will correspond to those observations with the most leverage (the most “outlying” points). We can then rewrite Eq. (18) as

$$\hat{\gamma} = \underset{\gamma}{\operatorname{argmin}} (1/2) \|y - Z\gamma\|_2^2 + \lambda_G \gamma^T G' \gamma + \sum_{j=1}^{p+n} w_j |\gamma_j| \quad (19)$$

$$Z = [X \ I_{n \times n}], \gamma = [\beta \ \alpha], w_j = \begin{cases} \lambda_1 & j = 1, \dots, p \\ \delta & j = p + 1, \dots, p + n, \end{cases}$$

$$G' = \begin{bmatrix} G & 0_{1 \times n} \\ 0_{n \times 1} & 0_{n \times n} \end{bmatrix} \in S_+^{(p+n) \times (p+n)},$$

where $S_+^{m \times m}$ is the set of positive semidefinite $m \times m$ matrices. This is just a GraphNet problem in an augmented set of $p + n$ variables, and so can be solved using the fast coordinate-wise descent methods discussed in the section “Optimization and computational considerations” below. After solving for augmented coefficients $\hat{\gamma}$ we can simply discard the last n coefficients to yield $\hat{\beta}$. A similar approach can be taken with the hinge-loss of a support vector machine classifier (as we show next),

or more generally with any loss function decomposable into an infimal convolution of convex functions (see Appendix A). The adaptive robust GraphNet is easily obtained by letting

$$w_j = \begin{cases} \lambda_1^* \hat{w}_j & j = 1, \dots, p \\ \delta & j = p+1, \dots, p+n \end{cases}$$

in Eq. (19) (see the section “Adaptive GraphNet regression” for more details on adaptive estimation).

Huberized Support Vector Machine (SVM) GraphNet for classification

In the $p \gg n$ classification problem, maximum-margin classifiers such as the support vector machine (SVM) often perform exceedingly well in terms of classification accuracy, but do not yield readily interpretable coefficients. For this reason we also developed a sparse SVM with graph constraints: the Support Vector GraphNet (SVGNet). This is related to the “Hybrid Huberized SVM” of Wang et al. (2008a), and is an alternative to the SPDA method. Using a “Huberized-hinge” loss function R_{HH} (see below) on the fit residuals, we have

$$\hat{\beta} = \kappa \operatorname{argmin} \mathcal{R}_{HH}(y^T X \beta; \delta) + \lambda_1 \|\beta\|_1 + \lambda_G \|\beta\|_G^2, \quad (20)$$

where $y \in \{-1, 1\}$, and letting $\hat{y} = X \hat{\beta}$ be the estimates of the target variable,

$$\mathcal{R}_{HH}(y, \hat{y}; \delta) = n^{-1} \sum_{i=1}^n L_\delta(y_i, \hat{y}_i) \quad (21)$$

$$\text{where } L_\delta(y_i, \hat{y}_i) = \begin{cases} (1 - y_i \hat{y}_i)^2 / 2\delta & \text{for } 1 - \delta < y_i \hat{y}_i \leq 1 \\ 1 - y_i \hat{y}_i - \delta/2 & \text{for } y_i \hat{y}_i \leq 1 - \delta \\ 0 & \text{for } y_i \hat{y}_i > 1, \end{cases}$$

which is the Huberized-hinge loss of Wang et al. (2008a). As with the Huber loss, there is an additional hyperparameter δ to be estimated or assumed. In this case, δ determines where the hinge-loss function switches from the quadratic to the linear regime (see Fig. 2a). This problem's loss function can also be written using infimal convolution to yield a more convenient quadratic objective term (see Appendix A).

Effective degrees of freedom for GraphNet estimators

Following results for the lasso (Zou et al., 2007) and the Elastic-Net (van der Kooij, 2007), the effective degrees of freedom df for the GraphNet regression are given by the trace of the “hat matrix” $H_{\lambda_G}(A)$ for the GraphNet estimator:

$$\hat{df} = \operatorname{tr}(H_{\lambda_G}(A)) = \operatorname{tr}\left(X_A \left(X_A^T X_A + \lambda_G G\right)^{-1} X_A^T\right),$$

where X_A denotes the columns of X containing just the “active set” (those variables with nonzero coefficients corresponding to a particular choice of λ_1). This quantity is very useful in calculating standard model selection criteria such as the Akaike Information Criterion (AIC), Bayesian Information Criterion (BIC), Mallows's C_p , and others. Importantly, it can also be used for the various GraphNet methods, as each of these is solved as an equivalent GraphNet problem (for example, Eq. (19)) for the adaptive robust GraphNet.

Rescaling coefficients to account for “double shrinking”

The Elastic-Net originally formulated by Zou and Hastie (2005) in both “naive” and rescaled forms. The authors noted that a combination of ℓ_1 and ℓ_2 penalties can “double shrink” the coefficients. To correct this they proposed rescaling the “naive” solution by a factor of $\kappa = 1 + \lambda_2$ (Zou and Hastie, 2005). Heuristically, the aim is to retain the desirable variable selection properties of the Elastic-Net while rescaling the coefficients to be closer to the original scale. However, as this result is derived for an orthogonal design, it is not clear that $\kappa = 1 + \lambda_2$ is the

correct multiplicative factor if the data are collinear, and this can complicate the problem of choosing a final set of coefficients. Following the arguments of Zou and Hastie (2005), for GraphNet regression we might rescale each coefficient by $\kappa_j = \hat{\Sigma}_{jj} + \lambda_G G_{jj}$ (see Eq. (28) and derivations in Appendix A) and where $\hat{\Sigma} = X^T X$. In the case of an orthogonal design and $G = I$ we would have $\hat{\Sigma} = I$ and thus $\kappa_j = 1 + \lambda_G$ —reducing to the Elastic Net rescaling employed in Zou and Hastie (2005).

A simpler alternative is to fit the Elastic-Net, generating a fitted response \hat{y} , and then to regress y on \hat{y} . In particular, solving the simple linear regression problem

$$y = \kappa \hat{y} = \kappa X \hat{\beta}, \kappa \in \mathbb{R}$$

yields an estimate $\hat{\kappa}$ that can be used to rescale the coefficients obtained from fitting the Elastic Net (Daniela Witten and Robert Tibshirani, personal communication). The intuitive motivation for this heuristic is that it will produce a $\hat{\kappa}$ that puts $\hat{\beta}$ and \hat{y} on a reasonable scale for fitting y .

Besides its simplicity, the principal advantage of this approach is that it requires no analytical knowledge about the amount of shrinkage that occurs as λ_G is increased. This is particularly appealing because the same strategy of regressing \hat{y} on y can be used with more general problems with more complicated forms, such as the adaptive robust GraphNet, where the additional shrinkage caused by the graph penalty can be corrected in this way.

Finally, we note that over-shrinking is not necessarily bad for classification accuracy. Indeed it may improve accuracy due to the rather complicated relationship between bias and variance in the classification (for an excellent discussion in the context of 0–1 loss see Friedman (1997)). The focus on recovering good estimates of coefficient magnitude in this section is thus most relevant to regression and to situations in which correct estimates of coefficient magnitude are important.

Interpreting GraphNet regression and classification

Interpreting GraphNet parameters: dual variables as prices

The GraphNet problem expressed in Eq. (5) derives from a constrained maximum likelihood problem, in which we want to maximize the likelihood of the parameters given the data, subject to some hard constraints on the solution—specifically, that they are sparse and structured (in the sense that their ℓ_1 and graph-weighted ℓ_2 norms are less than or equal to some constraint size). For concave likelihoods (as in generalized linear models and the cases considered above), this is a constrained convex optimization problem

$$\underset{\beta}{\text{maximize}} \quad \log \operatorname{lik}(\beta | X, y) \quad (22)$$

$$\text{subject to} \quad \|\beta\|_1 \leq c_1, \|\beta\|_G^2 \leq c_G, \quad (23)$$

where $c_1 \in \mathbb{R}_+$ and $c_G \in \mathbb{R}_+$ set hard bounds on the size of the coefficients in the ℓ_1 and ℓ_G norms, respectively. A standard approach for solving such problems is to relax the hard constraints to linear penalties (Boyd and Vandenberghe, 2004) and consider just those terms containing β , giving the “Lagrangian” form of the GraphNet problem

$$\hat{\beta} = \underset{\beta}{\operatorname{argmin}} \quad -\log \operatorname{lik}(\beta | X, y) + \lambda_1 \|\beta\|_1 + \lambda_G \|\beta\|_G^2, \quad \lambda_1, \lambda_G \in \mathbb{R}_+, \quad (24)$$

which contains a negative likelihood term that measures misfit to the data as well as the two penalties characteristic of GraphNet estimators.

In this Lagrangian formulation, the dual variables λ_1 and λ_G represent (linear) costs in response to a violation of the constraints. Since

we solve problem (24), c_1 and c_G are effectively zero, and we are penalized for any deviation of the coefficients from zero. This leads to one interpretation of λ_1 and λ_G : they are prices that we are willing to pay to improve the likelihood at the expense of a less sparse or less structured solution, respectively. For this reason, examining fit sensitivity to different values of λ_1 and λ_G tells us about underlying structure in the data. For example, if the task-related neural activity was very sparse and highly localized in a few uncorrelated voxels, then we should be willing to pay more for sparsity and less for smoothness (i.e., large λ_1 , small λ_G). In contrast, if large smooth and correlated regions underlie the task, then tolerating a large λ_G could substantially improve the fit. To explore such possibilities, we can plot test rates from cross validations at different combinations of parameters. Fig. 6 shows plots of median test classification rates as a function of λ_1 and λ_G over the parameter grid on which the various GraphNet classifiers were fit. We see that there are regions in the (λ_1, λ_G) parameter space that clearly result in better median classification test rates, corresponding to fits with particular levels of smoothness and sparsity.

Interpreting GraphNet coefficients

Problem (24) can also be arrived at from a Bayesian perspective as a maximum a posteriori (MAP) estimator. In this case, the form of the penalty $\mathcal{P}(\beta)$ is related to one's prior beliefs about the structure of the coefficients. For example, under the well-known equivalence of penalized regression techniques and posterior modes, the Elastic-Net penalty corresponds to the prior

$$p_{\lambda_1, \lambda_2}(\beta) \propto \exp\left\{-\left(\lambda_1 \|\beta\|_1 + \lambda_2 \|\beta\|_2^2\right)\right\}$$

(Zou and Hastie, 2005). The GraphNet penalty thus corresponds to the prior distribution

$$p_{\lambda_1, \lambda_G}(\beta) \propto \exp\left\{-\left(\lambda_1 \|\beta\|_1 + \lambda_G \beta^T G \beta\right)\right\} \propto \prod_{i=1}^p \exp\left\{-\lambda_1 |\beta_i|\right\} \prod_{i=1}^p \exp\left\{-\lambda_G \sum_{j \sim i} \beta_i G_{ij} \beta_j\right\}, \quad (25)$$

where $i \sim j$ denotes that node i in the graph G is adjacent to node j . Therefore, the GraphNet problems are also equivalent to a MAP estimator of the coefficients with a prior consisting of a convex combination of a global Laplacian (double-exponential) and a local Markov Random Field (MRF) prior. In other words, GraphNet methods explicitly take into account prior information about coefficients being globally sparse but locally structured by the graph G .

Optimization and computational considerations

Coordinate-wise descent and active set methods

Fitting regression methods to whole-brain fMRI data requires efficient computational methods, particularly when they must be cross-validated over a grid of possible parameter values. For instance, in the shopping example described in greater detail below (see the section “Application: predicting buying behavior using fMRI”), 26,630 input features (voxels) at each of 7 time points are used to classify future choices to purchase a product or not. Fitting the adaptive robust GraphNet using leave-one-subject-out (LOSO) cross-validation (i.e., 25 fits) for each realization of possible parameter values over this $90 \times 5 \times 6 \times 10 \times 3$ grid of possible parameters $\{\lambda_1, G, \lambda_G, \delta, \lambda_1^*\}$ requires 2,025,000 model fits on 1882 observations of 186,410 input features.

To efficiently fit GraphNet methods with millions of parameter combinations over hundreds of thousands of input features, we formulated the minimization problem (i.e., Eqs. (5), (15), and (20)) as a coordinate-wise optimization procedure (Tseng, 1988, 2001) using active set methods (Friedman et al., 2010). This approach fit one coefficient value at a time (“coordinate-wise” descent), holding the rest

constant, and kept an “active set” of nonzero coefficients. Fitting was initiated with a large value of λ_1 (corresponding to all coefficients being zero), and then slowly decreased λ_1 to allow more and more coefficients into the model fit. This procedure thus considered an “active set” of the model coefficients at each coordinate-wise update, rather than all 186,410 inputs. Occasional sweeps though all the coefficients were made to search for new variables to include, as in Friedman et al. (2010). Model fitting terminated before λ_1 reached zero, since fitting a fully dense set of coefficients is computationally expensive and known to produce poor estimates (Friedman et al., 2010; Hastie et al., 2009). Various heuristics and model selection criteria may be used for choosing a stopping point, for example, stopping once the AIC or BIC starts increasing significantly. AIC is known to be over-inclusive in model selection, and is therefore a more conservative stopping point.

Coordinate-wise descent is guaranteed to converge for GraphNet methods because they are all of the form

$$\argmin_{\beta} f(\beta_1, \dots, \beta_p) = \argmin_{\beta} g(\beta_1, \dots, \beta_p) + \sum_{j=1}^p h(\beta_j), \quad (26)$$

where $g(\beta_1, \dots, \beta_p)$ is a convex, differentiable function (e.g., squared-error or Huber loss plus the quadratic penalty $\|\beta\|_G^2$), and where each $h(\beta_j)$ is a convex (but not necessarily differentiable) function (e.g., the ℓ_1 penalty). If the convex, non-differentiable part of the penalty function is separable in coordinates β_j (as is true of $\|\beta\|_1 = \sum_{j=1}^p |\beta_j|$), then coordinate descent converges to a global solution of the minimization problem (Tseng, 2001). In the case of Huber loss or Huberized-hinge loss, the two-part loss function can be written as a single quadratic loss function using infimal convolution as described in the section “Huberized Support Vector Machine (SVM) GraphNet for classifications”. For instance, consider the coordinate-wise updates for the standard GraphNet problem given in Eq. (5). Letting $\hat{y} = \tilde{X} \tilde{\beta} + X_{\cdot j} \beta_j$ (where $\tilde{X} = X_{\cdot \neq j}$ is the matrix X with the j th column removed, and $\tilde{\beta} = \beta_{\neq j}$ the coefficient vector with the j th coefficient removed), the subdifferential of the risk with respect to only the j th coefficient (holding the others fixed) is

$$\partial_{\beta_j} \mathcal{R}_p = -X_{\cdot j}^T y + X_{\cdot j}^T \tilde{X} \tilde{\beta} + X_{\cdot j}^T X_{\cdot j} \beta_j + (\lambda_2/2) \tilde{\beta}^T (G_{\neq j})_{\cdot j} + \lambda_2 G_{jj} \beta_j + (\lambda_1/2) \Gamma(\beta_j), \quad (27)$$

where the set-valued function $\Gamma(\beta_j) = -1$ if $\beta_j < 0$, $\Gamma(\beta_j) = 1$ if $\beta_j > 0$ and $\Gamma(\beta_j) \in [-1, 1]$ if $\beta_j = 0$. If we let $\Gamma(\beta_j) = \text{sign}(\beta_j)$ in Eq. (27) (which is always a particular subgradient in the subdifferential of the risk), then the coordinate update iteration for the j th coefficient estimate is

$$\hat{\beta}_j \leftarrow \frac{S(X_{\cdot j}^T (y - \tilde{X} \tilde{\beta}) - (\lambda_2/2) \tilde{\beta}^T (G_{\neq j})_{\cdot j}, \lambda_1/2)}{X_{\cdot j}^T X_{\cdot j} + \lambda_2 G_{jj}}, \quad (28)$$

where

$$S(x, \gamma) = \text{sign}(x)(|x| - \gamma)_+ \quad (29)$$

is the elementwise soft-thresholding function (Donoho, 1995; Friedman et al., 2007a). Note that if graph $G = I$, and the columns of X are standardized to have unit norm, then the coordinate-wise Elastic-Net update is recovered (van der Kooij, 2007; Friedman et al., 2007b).

Computational complexity

A closer look at Eq. (28) reveals that if the variables are standardized (such that $X_{\cdot j}^T X_{\cdot j} = 1$) then the $(c+1)$ st coefficient update for the j th coordinate can be rewritten

$$\hat{\beta}_j^{(c+1)} \leftarrow S\left(\sum_{i=1}^N x_{ij} r_i^{(c)} + \hat{\beta}_j^{(c)} - (\lambda_2/2) \sum_{k \neq j} \beta_k G_{kj}, \lambda_1/2\right) / (1 + \lambda_2 G_{jj}), \quad (30)$$

where $r = y - \hat{y}$ is the vector of residuals. Letting m be the number of off-diagonal nonzero entries in G and initializing with $\hat{\beta}_j^{(0)} = 0$ for all j and $r^{(0)} = y$, the first sweep through all p coefficients will take $O(pn) + O(m)$ operations. Once a_1 variables are included in the active set, q iterations are performed according to Eq. (30) until the new estimates converge, at which point λ_1 is decreased incrementally and another $O(pn)$ sweep is made through the coefficients to find the next active set with a_2 variables (using the previous estimate as a warm start to keep q small). This procedure is repeated for l values of λ_1 , until the fit stops improving or a pre-specified coefficient density is reached. Let $a = \sum_{i=1}^l a_i$ denote the total number of coefficient updates over all l fits. The total computational complexity is then $O(lpn) + O(lm) + O(aq)$. Thus if G is relatively sparse (so m is small) and if it requires few iterations for coefficients in an active set to converge (q small)—which is true if the unpenalized loss function is quadratic—then the computational complexity is dominated by the $O(lpn)$ term representing the sweep through the coefficients necessary to find the next active set for each new value of λ_1 . We note that this suggests that including a screening procedure such as the STRONG rules (Tibshirani et al., 2012) could further speed up fitting in this context. Either making G dense or decreasing λ_1 until a becomes large can cause the other complexity terms to play a significant role and slow the speed of the algorithm. For example, if G is dense, then $m = p^2 - p$ and the $O(lm)$ term will dominate.

Cross validation, classification accuracy, and parameter tuning

For training and test data, trials for each subject were resampled within-subject to consist of 80 trials with exactly 40 purchases. If the subject originally had more than 40 purchases, sampling without replacement was used to select 40. If the subject originally had fewer than 40 purchases, sampling with replacement was used to select 40. Similar sampling was used to select exactly 40 trials without purchases. This resampling scheme ensured that the trials for each subject were balanced between purchasing and not purchasing. Further, because our cross-validation schemes defined folds on the subject level, this ensured that every training and test set in the cross-validation was also balanced.

For the cross-validation, ranges of parameter values were chosen based on a few preliminary fits and these ranges used to define a "grid" of parameters values on which to fit the various models. This parameter grid was very large and with the refitting involved in cross-validation, resulted in millions of fits. The smoothness of the rates as a function of the parameters (see Fig. 6) suggests that smaller grids are likely better suited to most applications, and we anticipate that more efficient adaptive approaches to parameter search—such as focused grid search methods (Jimenez et al., 2009) or sampling methods inspired by Bayesian approaches to similar problems—will ultimately prove superior. We leave these refinements to future work. The grid values used here are given in Appendix A.

In order to choose a final set of coefficient estimates from multiple fits across cross-validation folds, we took the element-wise median of the coefficient vectors across the folds. Thus a feature corresponding to a particular voxel at a particular TR would have to appear (be non-zero) in more than half of the 25 cross-validation folds in order to be included in the final coefficient estimate used in the out-of-sample (OOS) analysis. There are several justifications for taking the median across folds: (1) the median preserves sparsity, (2) the median is the appropriate maximum likelihood estimator for the double-exponential (Laplacian) distribution that corresponds to the ℓ_1 sparsity prior on the coefficients (see discussion in Groseknick et al., 2008), (3) such a procedure is closely related to the Median Probability Model, which is the model consisting of those variables that have posterior probability ≥ 0.5 of being in a model, and which has been shown to have optimal predictive performance for linear models (Barbieri and Berger, 2004), and (4) it is similar to other recently-developed model selection procedures for sparse models such as Stability Selection (Meinshausen and Bühlmann,

2010) that use the number of times a variable appears across multiple sparse fits to resampled data in order to significantly improve model selection. Further, we have found this approach to be quite effective in practice (see the out-of-sample results that follow). Note that such inclusion of a variable only if it appears in more than half of the 25 cross-validation folds is a natural means of imposing some "reliability" or "stability" on the coefficients.

Application: predicting buying behavior using fMRI

Subjects and SHOP task

Data from 25 healthy right-handed subjects were analyzed (Knutson et al., 2007). Along with the typical magnetic resonance exclusions (e.g., metal in the body), subjects were screened for psychotropic drugs, cardiac drugs, ibuprofen, substance abuse in the past month, and history of psychiatric disorders (DSM IV Axis I) prior to collecting informed consent. Subjects were paid \$20.00 per hour for participating and also received \$40.00 in cash to spend on products. Of 40 total subjects, 6 subjects who purchased fewer than four items per session (i.e., <10%) were excluded due to insufficient data to fit, 8 subjects who moved excessive amounts (i.e., >2 mm between whole brain acquisitions) were excluded, and one subject's original fMRI data could not be recovered and so were omitted, yielding the final total of 25 subjects included in the analysis.

While being scanned, subjects participated in a "Save Holdings Or Purchase" (SHOP) task (Fig. 3). During each task trial, subjects saw a labeled product (product period; 4 s), saw the product's price (price period; 4 s), and then chose either to purchase the product or not (by selecting either "yes" or "no" presented randomly on the right or left side of the screen; choice period; 4 s), before fixating on a crosshair (2 s) prior to the onset of the next trial (see Fig. 3).

Each of 80 trials featured a different product. Products were pre-selected to have above-median attractiveness, as rated by a similar sample in a pilot study. While products ranged in retail price from \$8.00 to \$80.00, the associated prices that subjects saw in the scanner were discounted down to 25% of retail value to encourage purchasing. Therefore the cost of each product during the experiment ranged from \$2.00 to \$20.00. Consistent with pilot findings, this led subjects to purchase 30% of the products on average, generating sufficient instances of purchasing to fit.

To ensure subjects' engagement in the task, two trials were randomly selected after scanning to count "for real". If subjects had chosen to purchase the product presented during the randomly selected trial, they paid the price that they had seen in the scanner from their \$40.00 endowment and were shipped the product within two weeks. If not, subjects kept their \$40.00 endowment. Based on these randomly drawn trials, seven of twenty-five subjects (28%) were actually shipped products.

Subjects were instructed in the task and tested for comprehension prior to entering the scanner. During scanning, subjects chose from 40 items twice and then chose from a second set of 40 items twice (80 items total), with each set presented in the same pseudo-random order (item sets were counterbalanced across subjects). We consider only data from the first time each item was presented here (see Groseknick et al. (2008) for a comparison between first and second presentations). After scanning, subjects rated each product in terms of how much they would like to own it and what percentage of the retail price they would be willing to pay for it. Then, two trials were randomly drawn to count "for real", and subjects received the outcome of each of the drawn trials.

A second validation sample included 17 healthy right-handed subjects (Karmarkar et al., submitted for publication). These subjects passed the same screening, inclusion, and exclusion criteria. Of an original sample of 24, 6 subjects purchased fewer than four items per session, and one showed excessive motion. These subjects were excluded from analyses, as before. Subjects also received the same payment and underwent the same scanning and experimental



Fig. 3. Save Holdings, or Purchase (SHOP) task trial structure. Images represent what the subject saw, bars represent 2 s TRs (T1–T7). Subjects saw a labeled product (product period; 4 s, 2 TRs), saw the product's price (price period; 4 s, 2 TRs), and then chose either to purchase the product or not (by selecting either “yes” or “no” presented randomly on the right or left side of the screen; choice period; 4 s, 2 TRs), before fixating on a crosshair (2 s, 1 TR) prior to the onset of the next trial.

procedures. Importantly, however, subjects were different individuals who were exposed to different products, and were scanned more than three years after the original study.

Image acquisition

Functional images were acquired with a 1.5 T General Electric MRI scanner using a standard birdcage quadrature head coil. Twenty-four 4-mm-thick slices (in-plane resolution 3.75×3.75 mm, no gap) extended axially from the midpons to the top of the skull, providing whole-brain coverage and adequate spatial resolution of subcortical regions of interest (e.g., midbrain, NAcc, OFC). Whole-brain functional scans were acquired with a T2*-sensitive spiral in-/out- pulse sequence (TR = 2 s, TE = 40 ms, flip = 90°), which minimizes signal dropout at the base of the brain (Glover and Law, 2001). High-resolution structural scans were also acquired to facilitate localization and coregistration of functional data, using a T1-weighted spoiled grass sequence (TR = 100 ms, TE = 7 ms, flip = 90°).

Preprocessing

After reconstruction, preprocessing was conducted using Analysis of Functional Neural Images (AFNI) software (Cox, 1996). For all functional images, voxel time-series were sinc interpolated to correct for non-simultaneous slice acquisition within each volume, concatenated across runs, corrected for motion, and normalized to percent signal change with respect to the voxel mean for the entire task. For further preprocessing details see (Grosenick et al., 2008). Given that spatial blur would artificially increase correlations between variables for the voxel-wise analysis, we used data with no spatial blur and a temporal high pass filter for all analyses. Note that in general, smoothing before running analyses will compound the problems with correlation mentioned above, resulting in “rougher” (high-frequency) coefficients overall (see discussion in (Hastie et al., 1995)).

Spatiotemporal data were arranged as in previous spatiotemporal analyses (Mourão-Miranda et al., 2007). Specifically, data were arranged as an $n \times p$ data matrix X with n corresponding to the number of trial observations on the p input variables, each of which was a particular voxel at a particular time point. This yielded 26,630 voxels taken at 7 time points (each taken every 2 s), yielding a total of $p = 186,410$ input features per trial. Altogether, the data used for training and test from (Knutson et al., 2007) included $n = 1882$ trials across the 25 subjects. The validation sample from (Karmarkar et al., submitted for publication) included $n = 322$ trials across the 17 subjects. In the first case (training and testing on the Knutson et al. (2007) data), the number of ‘buy’ trials was upsampled to match the number of ‘not buy’ trials in order to efficiently use the data when fitting the models. In the out-of-sample (OOS) validation on the (Karmarkar et al., submitted for publication) data, however, the number of ‘not buy’ trials were downsampled to match the smaller

number of ‘buy’ trials in order to be more conservative in estimating the out-of-sample accuracy (and related p -values).

Results

Classification rates

If neural substrates implicated in choice show invariance across individuals, a method that successfully identifies and uses these substrates to predict choice should generalize well across subjects. We compared the GraphNet classifier accuracies with accuracies obtained using linear SVM (where accuracy in this case is the ability to correctly predict a subject's choices to purchase a product or not). In particular we looked at generalization of fits to held-out “test” sets (consisting of subjects held out of a particular stage of the cross validation procedure, but still present in other cross-validation stages), and to out-of-sample (OOS) data (new data never used at any stage of the model fitting) consisting of different subjects from another study (Karmarkar et al., submitted for publication). Results and model parameters for the GraphNet classifiers and linear SVM across the 25 subjects from Knutson et al. (2007) (“Training”, “Test”) and 17 subjects from Karmarkar et al. (submitted for publication) (“OOS”) are listed in Tables 1 and 2, as well as a summary of each method's properties. Models were fit using either leave-one-subject-out (LOSO, Table 1) or leave-5-subjects-out (L5SO, Table 2) cross-validation, and both training and test results are displayed to allow comparison of overfitting on the training data versus the held-out test data. As cross-validation is known to yield an overly optimistic estimate of the true classification error rate (Hastie et al., 2009), model fits to the initial data set ($n = 25$; Knutson et al. (2007)) were tested on out-of-sample (OOS) data ($n = 17$; Karmarkar et al. (submitted for publication)) collected more than three years later using different subjects shown different products. These out-of-sample results provide the most rigorous demonstration of fit generalization to new data, adjusting for any overfitting by the cross-validation procedure, and are the strongest evidence for invariance in the neural representation of choice across subjects. The p -values reported correspond to these out-of-sample accuracies on $n = 322$ trials across the 17 new subjects.

Generalization to held-out groups (L5SO cross-validation)

Best median training, median test, and out-of-sample (OOS) rates are described for GraphNet classifiers fit over the grid of parameters given in Eq. (32). The linear SVM parameters are also given in Eq. (32). Despite a more than 1000-fold increase in the number of input features relative to earlier volume of interest (VOI) analyses (Grosenick et al., 2008), whole-brain classifiers performed significantly better than previous VOI-based predictions fit to the same data

Table 1

Median classification accuracy and parameters for SPDA and SVM classifiers fit with leave-5-subjects-out (L5SO) cross validation.

Classification accuracy					Model type				
Method	Training	Test	OOS	p-Value [†]	Sparse	Tikhonov	Structured	Robust	Adaptive
					(λ_1)	(λ_2)	(λ_C)	(δ)	(λ_1^*)
Linear SVM ^a	97.9%	71.0%	65.8%	2.7×10^{-8}		$^{\dagger\dagger}3.8 \times 10^{-6}$		✓	
Lasso ^b	98.8%	68.5%	58.4%	0.003	33				
Elastic Net ^c	90.4%	72.5%	64.3%	3.3×10^{-7}	54	10000			
GraphNet ^d (GN)	86.9%	73.7%	64.6%	1.8×10^{-7}	68	1000	100		
Robust GN (RGN)	86.8%	74.5%	64.9%	1.8×10^{-7}	43	100	100	0.3	
RGN + temporal	96.5%	73.8%	63.0%	5.7×10^{-6}	42	1000	10	0.5	
Adaptive RGN	91.4%	73.8%	67.1%	8.6×10^{-10}	50	10000	100	0.4	0.01
ARGN + temporal	90.8%	73.5%	66.8%	1.8×10^{-9}	40	1000	100	0.3	0.01
Support Vector GN	85.3%	73.0%	62.4%	1.6×10^{-5}	120	1000	10	0.5	

OOS is short for “out-of-sample”. Chance level is 50%. The maximum accuracy in each column is bolded. [†]p-Value is calculated for the out-of-sample accuracy using an exact test for the probability of success in a Bernoulli experiment with $n = 322$ trials with success probability of 0.5. ^{††}This is the C parameter for the SVM. ✓The linear SVM is robust as a result of its hinge loss function, which does not have a parameter δ associated with it.

^a (Cortes and Vapnik, 1995).

^b (Tibshirani, 1996).

^c (Zou and Hastie, 2005).

^d (Grosenick et al., 2009b).

(Grosenick et al., 2008; Knutson et al., 2007). Further, among these whole-brain classifiers, adaptive and robust methods performed best on out-of-sample data. SVGN performed similarly to the linear SVM (but unlike linear SVM, yields structured, sparse coefficients that aid interpretability). Further, Lasso and linear SVM tended to overfit the training data more than the SPDA-GraphNet classifiers, as evidenced by their higher training but lower test rates. Overall, the adaptive robust GraphNet classifier showed the best out-of-sample classification rate, with accuracy on new data of 67.1% (for comparison, the linear SVM accuracy was 65.8%). Examining the distribution of test classification rates across the 25 folds (25 sets leaving 5 subjects out), Fig. 4b shows that the linear SVM appears to have less variance across test fits to held-out subjects. The marked non-normality of these distributions is interesting, and motivated us to report median rather than mean accuracy over cross-validation folds.

Generalization to held-out individuals (LOSO cross-validation)

In addition to the leave-5-subjects out (L5SO) cross-validation, we also ran leave-one-subject-out (LOSO) cross validation (i.e., using the data from 24 subjects to predict results for each remaining subject). Repeating this procedure for all subjects yielded one held-out classification rate per subject, indicating how well the group fit generalized to that subject. Repeating this for all subjects yielded one held-out test rate per subject. This rate indicated how well the model fit

based on all but one subjects' data generalized to the held-out subject—a measure of invariance across subjects as well as a quantity that may be of interest in studies of individual differences. Fig. 4a shows smoothed histograms of the LOSO classification rates for the robust GraphNet, adaptive robust GraphNet, SVGN, and linear SVM classifiers. Overall, the GraphNet classifiers outperform the linear SVM on LOSO cross-validation across subjects. When the LOSO fits were used to classify choice out-of-sample, the adaptive robust GraphNet classifier again yielded the best performance, now at almost 70% classification accuracy. LOSO cross-validation appears to result in better OOS generalization than L5SO cross-validation for these data. More important than the improvement in classification performance, however, is the greater interpretability of these methods.

Visualization and interpretation of coefficients and parameters

Interpreting GraphNet coefficients

While GraphNet classifiers and linear SVM both classified purchase choices successfully, the GraphNet-based classifiers produced more interpretable results. Consistent with previous VOI-based analyses, the GraphNet, robust GraphNet classifier (Fig. 5), and adaptive robust GraphNet (Fig. 5) classifiers all identified similar regions to those chosen as VOIs (Knutson et al., 2007), with coefficients present at the time points corresponding to peak discrimination in the VOI time-series

Table 2

Median classification accuracy and parameters for SPDA and SVM classifiers fit with leave-one-subject-out (LOSO) cross validation.

Classification accuracy					Model type				
Method	Training	Test	OOS	p-Value [†]	Sparse	Tikhonov	Structured	Robust	Adaptive
					(λ_1)	(λ_2)	(λ_C)	(δ)	(λ_1^*)
Linear SVM ^a	91.6%	68.8%	65.2%	9.7×10^{-8}		$^{\dagger\dagger}7.6 \times 10^{-6}$		✓	
Lasso ^b	90.5%	68.8%	61.2%	7.1×10^{-5}	63				
Elastic Net ^c	90.8%	70.0%	63.0%	5.7×10^{-6}	61	1000			
GraphNet ^d (GN)	87.5%	71.3%	67.7%	4.1×10^{-10}	54	10000	1000		
Robust GN (RGN)	83.8%	72.5%	67.4%	4.1×10^{-10}	25	10	100	0.2	
RGN + temporal	83.8%	72.5%	67.1%	8.6×10^{-10}	55	100	1000	0.6	
Adaptive RGN	85.4%	72.5%	69.8%	1.7×10^{-12}	20	10	1000	0.2	0.01
ARGN + temporal	88.3%	73.8%	68.9%	2.0×10^{-11}	30	1000	100	0.2	0.01
Support Vector GN	89.5%	73.8%	65.2%	9.7×10^{-8}	84	100	100	0.5	

OOS is short for “out-of-sample”. Chance level is 50%. The maximum accuracy in each column is bolded. [†]p-Value is calculated for the out-of-sample accuracy using an exact test for the probability of success in a Bernoulli experiment with $n = 322$ trials with chance level at 50%. ^{††}This is the C parameter for the SVM. ✓The linear SVM is robust as a result of its hinge loss function, which does not have a parameter δ associated with it.

^a (Cortes and Vapnik, 1995).

^b (Tibshirani, 1996).

^c (Zou and Hastie, 2005).

^d (Grosenick et al., 2009b).

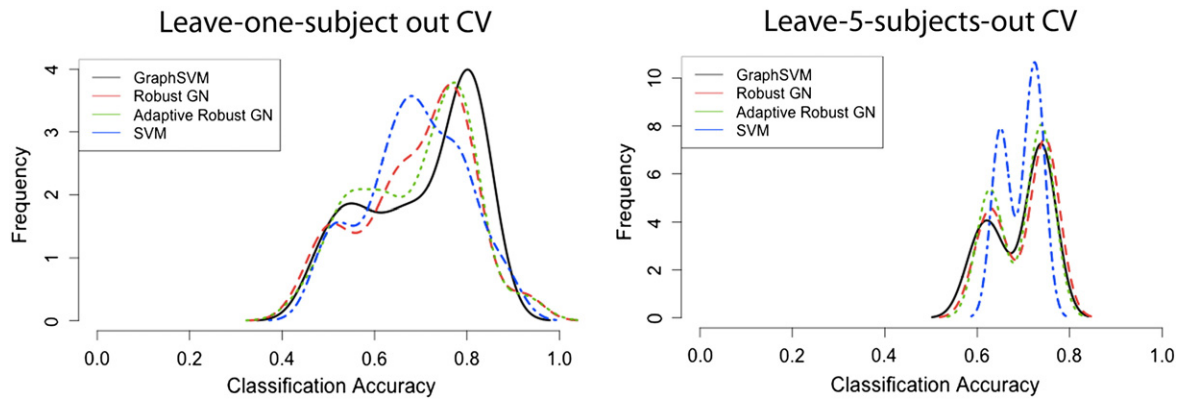


Fig. 4. (Left) Smoothed histogram densities of leave-one-subject out (LOSO) accuracy rates on test data. Models were fit to all subjects except one, and then tested on the held-out subject. This was done for all subjects and smoothed histograms of these rates were calculated for the best fitting models. (Right) The same procedure was repeated, but leaving 5 subjects out at a time for a total of 25 cross-validation folds. Both plots show some bimodality suggestive of different underlying groups.

(Knutson et al., 2007) and VOI classification (Grosenick et al., 2008). In particular, nucleus accumbens (NAcc) activation began to positively predict purchase choices at the time of product presentation, and this prediction persisted throughout subsequent price presentation. Medial prefrontal cortex (MPFC) and midbrain activation, on the other hand, began to positively predict purchase choices at the onset of price presentation (but not during previous product presentation). Additionally—and not included in any previous findings—posterior cingulate activation also began to robustly and positively predict purchase choices during price presentation. Reassuringly, no regions' activation predicted purchase choices during fixation presentation. Interestingly, the best fits chose far more voxels that positively predicted than negatively predicted purchasing.

Together, these findings demonstrate that sparse, structured, whole-brain methods like GraphNet can facilitate the discovery of new behaviorally relevant spatiotemporal neural activity patterns that existing VOI-based methods miss. Due to the temporal and spatial structure of these data and the experimental design, it was possible not only to localize brain activity that predicted purchasing choices, but also to clearly observe the temporal evolution of predictive activity throughout the brain. That is, by fitting whole-brain models across multiple time points corresponding to a structured design (and accounting for the hemodynamic response) we could evaluate over time which temporal aspects of the experimental design related to which sets of predictive coefficients across the brain. The fact that coefficient vectors estimated from the Knutson et al. (2007) data could be used to accurately predict choices of new subjects shown different products several years later speaks to the stability of the neural activity related to the task across subjects and products, and to the quality of the model.

Interpreting GraphNet parameters

Fig. 6 shows plots of median L5SO cross-validation rates over the values $\{\lambda_1, \lambda_G, G\}$ (28) on which we fit the four GraphNet classifiers (other parameters are set to the values shown in Table 1; plots for LOSO rates are similar). In all cases, there is a region in the interior of the explored parameter space $\{\lambda_1, \lambda_G, G\}$ in which the models empirically perform best. In all cases this region involves both smoothing and some level of sparsity, and the classifiers built with lasso (L) and Elastic-Net (EN)—shown as separate bars for the GraphNet (GN) fits—underperform relative to the sparse and smooth GraphNet classifiers on these data. Comparison of the rates in Fig. 6 suggests that a certain amount of coefficient smoothness and inclusion of correlated variables in the final fit is important for this data set, and that using a robust loss function tightens the region of optimal parameter performance.

Discussion and conclusions

Interpretable models for whole-brain spatiotemporal fMRI

We sought to design and develop a novel classification method for fMRI data that could fulfill several aims. First, the method should deliver interpretable results for whole-brain data over multiple time-points in the native data space. Second, the method should yield classification accuracy (or goodness-of-fit) competitive with current state-of-the-art multivariate methods. Third, the method should choose relevant features in a principled and asymptotically consistent way (i.e., it should include relevant features while excluding nuisance parameters). Fourth, the method should accommodate flexible constraints on model coefficients related to prior information (e.g., local smoothness, connectivity). Fifth, the method should remain robust to outliers in the data. Sixth, the method should generate coefficients with relatively unbiased magnitudes (despite employing shrinkage methods to yield sparsity). And seventh (and finally), the method should have the capacity to detect a range of possible signals, from smooth and localized to sparse and distributed.

The GraphNet-based methods presented here make a first step toward meeting these desirable (and often competing) aims. In particular, the adaptive robust GraphNet allows automatic variable selection (Zou and Zhang, 2009), incorporation of prior information in the form of a graph penalty, and yields minimally biased and asymptotically consistent coefficient estimates as a result of adaptive reweighting. Robust GraphNet methods can be applied to either regression or classification settings (using Optimal Scoring), and generate classification rates that compete favorably with state-of-the-art multivariate classifiers. The tuning parameters (λ_1, λ_G) and the graph G allow for a diversity of sparse and smooth data, and the relationship of model fits to these parameters provides information about the structure of the detected signal.

Choice in the context of purchasing admittedly represents only one application, and future validation on additional data sets is necessary. However, in this context the GraphNet classifiers generalize well to independent experiments involving purchasing (i.e. when fit to new data collected years after the experiments originally used to train the models, with different subjects and different products). Adaptive robust GraphNet methods showed the best out-of-sample generalization, and generated parsimonious, interpretable models. It is worth noting that the models that did best when fit to the in-sample cross-validation test folds were not best when fit to the out-of-sample data. This suggests that the overfitting, or “optimism”, known to exist in cross-validation (Hastie et al., 2009) can affect models differently, and that a true out-of-sample prediction is necessary to accurately assess which models generalize best.

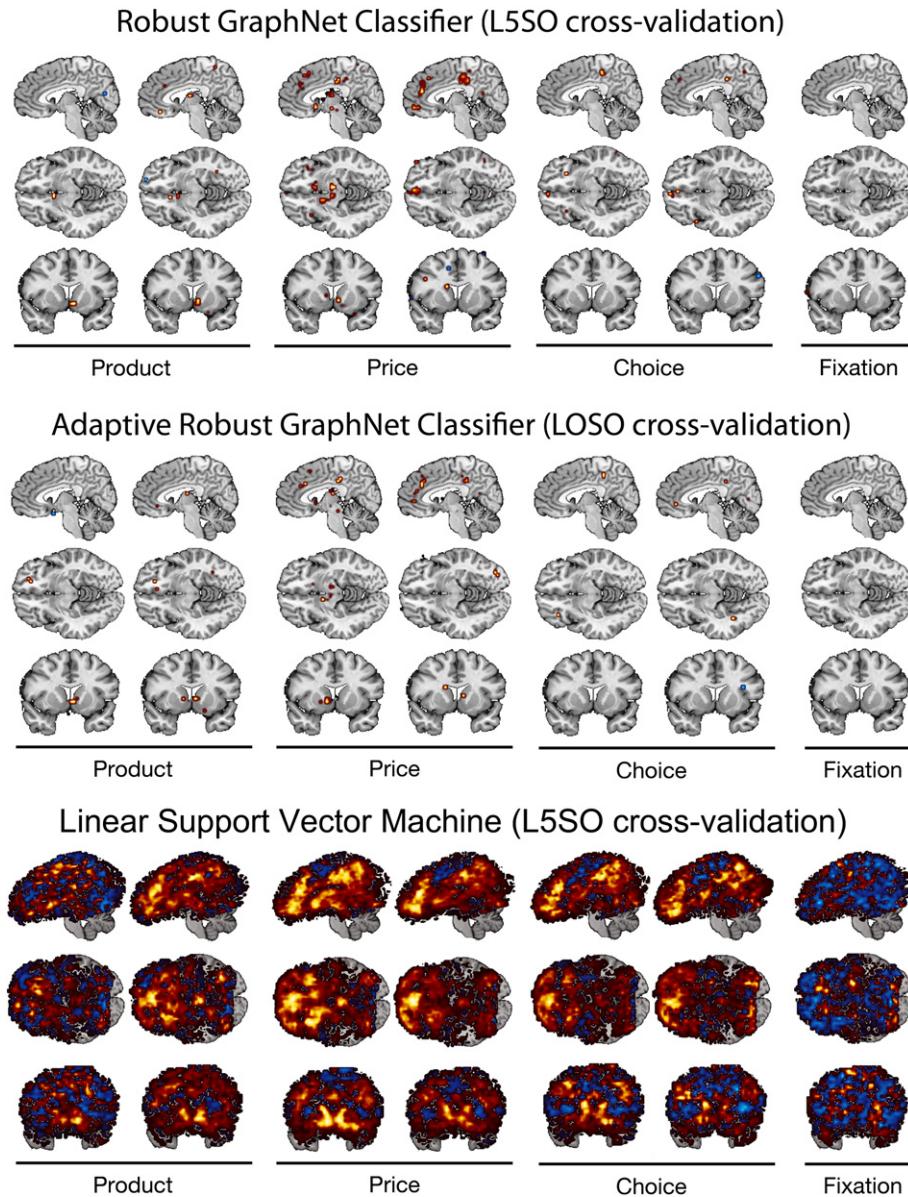


Fig. 5. Whole-brain classification results from the SHOP task (see Fig. 3 for task structure). (Top) Median coefficient maps from the best robust GraphNet classifier (median test accuracy of 74.5% over cross-validation folds and out-of-sample accuracy of 64.9%) fit using Leave-5-subjects-out (L5SO) cross-validation are shown at two time points for product, price, and choice periods, as well as the fixation period. Warm colored coefficients denote areas that predict purchasing a product, while cool-colored areas those that predict not purchasing. The areas chosen by the robust GraphNet classifier highlight regions suggested by previous studies including the bilateral nucleus accumbens (NAcc) and the mesial prefrontal cortex (MPFC) (Groseknick et al., 2008; Knutson et al., 2007), but also implicate new regions including the anterior cingulate and posterior cingulate cortices. (Middle) Similar plots for the best adaptive robust GraphNet classifier (median test accuracy of 72.5% over cross-validation folds; out-of-sample accuracy of 69.8%) fit using leave-one-subject (LOSO) cross-validation. Although the solution is sparser, the regions chosen remain the same. (Bottom) Coefficients for the best linear SVM (median test accuracy of 71% over cross-validation folds; out-of-sample accuracy of 65.8%) fit using Leave-5-subjects-out (L5SO) cross-validation for comparison.

In summary, we have developed a family of robust, adaptive, and interpretable methods that can be fit efficiently to large data sets over large parameter grids. This method will allow investigators to search in a data-driven fashion across the whole brain and multiple time points, obviating the need for volume-of-interest based approaches in fMRI classification and regression, and providing an effective alternative to mass-univariate approaches for whole-brain analysis.

Application to SHOP task data

In the context of predicting human behavior from brain data, the current whole brain methods offer clear advantages over previous volume of interest based methods. In terms of classification accuracy, previous work on the Knutson et al. (2007) data has resulted in cross-

validated test rates of 60% (with a leave-one-out cross validation using logistic regression on VOI-averaged data; see Knutson et al. (2007) for details), and 67% (with a 5×2 cross validation using SPDA-Elastic Net on VOI voxel data; see Groseknick et al. (2008) for details). Here, using the same preprocessing and data as in these previous VOI-based approaches, but using GraphNet classifiers on whole-brain data, we achieve test rates from 73.0 to 74.5% for L5SO cross validation and 71.3 to 73.8% for LOSO cross validation. Further, out-of-sample (OOS) rates for the GraphNet classifiers were 67.1% (L5SO) and 69.8% (LOSO). Thus, in this case, even out-of-sample rates with GraphNet classifiers outperform in-sample cross validation test rates on VOI-based classifiers—a considerable improvement. In taking classification accuracy as a measure of goodness-of-fit, this indicates that GraphNet classifiers result in better fits and improved generalization relative to VOI methods, and suggests that the resulting coefficients are a good

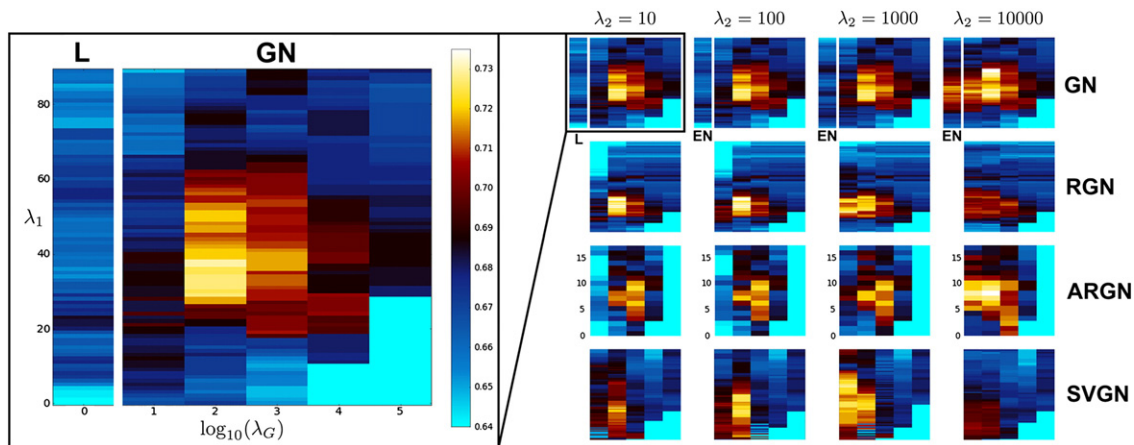


Fig. 6. Examples of classification accuracy (test) plotted as a function of penalty parameters. The blown up image on the left shows an image of the median test accuracy rates for the GraphNet SPDA classifier (GN) as functions of hyperparameters λ_1 and λ_G (with $\lambda_2 = 0$). Warm colors indicate median classification rates above 70% (for L5SO cross-validation) and cool colors median accuracy below 70% (see color bar for scale). The separate column (L) indicates the standard Lasso solution at $\lambda_G = 0$. There is a clear maxima at $\lambda_1 = 40$, $\lambda_G = 100$. The smaller images on the right show similar plots for the GraphNet (GN), Robust GraphNet (RGN), Adaptive Robust GraphNet (ARGN), and Support Vector GraphNet (SVGN) classifiers at four values of the graph G diagonal scale λ_2 . Note the different scale on the ARGN models. It is of some interest that all the plots are rather slowly varying in the parameters and demonstrate significantly unimodal peaks (neither of these need be the case).

representation of invariant features that discriminate between choosing to purchase or not across subjects and products.

Turning to examine the coefficients, we see that the GraphNet classifiers reassuringly deliver findings consistent with prior volume of interest based results (Groseknick et al., 2008; Knutson et al., 2007), replicating the observation that nucleus accumbens (NAcc) activation begins to predict purchase choices during product presentation while medial prefrontal cortical (MPFC) activation begins to predict purchase choices during price presentation. It is also interesting to note areas that were not included by previously applied methods and might not have been noticed if not for the whole-brain analysis (and which might help account for the improved classification rates over previous VOI analyses).

While one account posits that in the context of fMRI, NAcc activation indexes gain predictions (Knutson and Greer, 2008; Knutson et al., 2001), an alternative account posits that NAcc activation instead indexes gain prediction errors (e.g., Hare et al., 2008). To the extent that gain predictions forecast future events while gain prediction errors are adjustments of those forecasts after an error is detected, the gain prediction account posits that NAcc activation in response to products should predict subsequent purchase choices. Applied to SHOP task data, the GraphNet classifier results clearly support the gain prediction functional account of NAcc activity, since NAcc activation in response to products predicts future choices to purchase, whereas MPFC activity does not. Instead, MPFC activity predicts choice in response to later presented price information, consistent with a value integration account (Knutson et al., 2005; Fig. 5). The GraphNet classifiers also revealed a previously unnoticed result in which anterior and posterior cingulate activity clearly predicts purchase choices at price presentation (Fig. 5). Accounts of cingulate function in the context of purchasing remain less developed than similar accounts of NAcc and MPFC function. Nonetheless, this result might be consistent with attentional and salience-based accounts of posterior cingulate function (McCoy et al., 2003), and highlights a region that deserves further investigation in the context of choice prediction.

Future directions

GraphNet methods can be further optimized, opening new avenues for exploration. For instance, investigators might compare graph constraints other than those related to just spatial-temporal adjacency, including (1) weighted graphs derived from the data to adapt to local smoothness, (2) cut-graphs derived from segmented brain

atlases that allow adjacent but functionally distinct regions to be independently penalized, and (3) weighted graphs derived from structural data, which would allow constraints on voxels adjacent on a connectivity graph, rather than in space or time (see Ng et al. (2012) for a promising step in this direction). Further, investigators might use the goodness-of-fit measure provided by GraphNet to infer which of a set of structural graphs best relates to functional data, or to adaptively alter graph weights to explore structure in functional data (in a Variational Bayes framework, for example).

All of the methods considered above assume linear relationships between input features and target variables. While this assumption suffices in many cases, signal saturation effects alone suggest that it might not faithfully mirror underlying physiological signals. Nonlinear methods based on scatterplot smoothers have recently been developed and shown to work well in combination with coordinate-wise methods (Ravikumar et al., 2009), and previous work applying sparse regression to features derived using factor analysis have yielded promising results (Groseknick et al., 2009a; Wager et al., 2011). Investigators might thus combine nonlinear methods with sparse structured feature selection methods (Allen et al., 2011) to generate more flexible and accurate, yet still interpretable, models of brain dynamics. Finally, we note that because we are operating directly on voxel data, we are working in the “native” reconstructed 3D data space rather than on factors derived from these data or on a dictionary of basis functions that approximate features of the data (e.g., wavelets). Certainly, the optimization scheme described here would also extend to solving problems using features derived from the data, and it is an interesting direction for future research to explore GraphNet penalties in these other contexts and to compare GraphNet methods to existing regression and classification methods that operate on lower dimensional embeddings or dictionary representations of the data. Whether operating directly on the data with sparse structured methods or on derived features is more appropriate will depend on the application. The methods presented here demonstrate that the former approach can be quite effective, and provides results that are easily interpreted in the native data space.

Appendix A. Robust GraphNet: coordinate-wise coefficient updates using infimal convolution

Algorithm 1. Robust GraphNet update using infimal convolution

1. Given a set of data and parameters $\Omega = \{X, y, \lambda_1, \lambda_G\}$, previous coefficient estimates $\hat{\alpha}^{(r)}, \hat{\beta}^{(r)}$, and $p \times p$ positive semidefinite constraint graph $G \in S_+^{p \times p}$, let

$$\hat{\gamma}^{(r)} = [\hat{\beta}^{(r)} \hat{\alpha}^{(r)}]^T$$

$$Z = [X \ I_{n \times n}].$$

2. Choose coordinate j using essentially cyclic rule (Tseng, 2001) and fix $\tilde{\gamma} = \{\gamma_k^{(r)} | k \neq j\}$, $\tilde{Z} = Z_{\cdot, \neq j}$, $\tilde{\beta} = \{\beta_k^{(r)} | k \neq j\}$
3. Update $\hat{\gamma}_j^{(r)}$ using

$$\hat{\gamma}_j^{(r+1)} \leftarrow \begin{cases} \frac{S(Z_j^T(y - \tilde{Z}\tilde{\gamma}) - (\lambda_2/2)\tilde{\gamma}^T(G'_{\neq j})_j, \lambda_1/2)}{Z_j^T Z_j + \lambda_G G'_{jj}} & \text{if } j \in \{1, \dots, p\} \\ S((y - \tilde{Z}\tilde{\gamma})_j, \lambda_1/2) & \text{if } j \in \{p+1, \dots, p+n\}, \end{cases}$$

where $S(x, \lambda)$ is the element-wise soft-thresholding operator in Eq. (29), and where G' is the appropriately augmented G given in Eq. (19). For adaptive version replace λ_1 with $\lambda_1^* \hat{w}_j$ in above update (see the section “Adaptive GraphNet regression”).

4. Repeat steps (1)–(3) cyclically for all $j \in \{1, \dots, p+n\}$ until convergence (see discussion of convergence in Friedman et al. (2007a)).
5. Optional: rescale resulting estimates using method from the section “Rescaling coefficients to account for “double shrinking””.

Derivation of updates in Algorithm 1

For a particular coordinate j , we are interested in the estimates

$$\hat{\gamma}_j = \underset{\gamma_j}{\operatorname{argmin}} (1/2) \|y - \tilde{Z}\tilde{\gamma} - Z_j \gamma_j\|_2^2 + \lambda_G (\tilde{\gamma}^T (G'_{\neq j})_j \gamma_j + G'_{jj} \gamma_j^2) + \lambda_1 |\gamma_j| \text{ if } j \in \{1, \dots, p\},$$

$$\hat{\gamma}_j = \underset{\gamma_j}{\operatorname{argmin}} (1/2) \|y - \tilde{Z}\tilde{\gamma} - Z_j \gamma_j\|_2^2 + \delta |\gamma_j| \text{ if } j \in \{p+1, \dots, p+n\}.$$

By the arguments in the section “Coordinate-wise descent and active set methods”, this yields the coordinate-wise updates

$$\hat{\gamma}_j \leftarrow \frac{S(Z_j^T(y - \tilde{Z}\tilde{\gamma}) - (\lambda_2/2)\tilde{\gamma}^T(G'_{\neq j})_j, \lambda_1/2)}{Z_j^T Z_j + \lambda_G G'_{jj}} \text{ if } j \in \{1, \dots, p\},$$

$$\hat{\gamma}_j \leftarrow \frac{S(Z_j^T(y - \tilde{Z}\tilde{\gamma}), \lambda_1/2)}{Z_j^T Z_j} \text{ if } j \in \{p+1, \dots, p+n\},$$

where $S(x, \lambda)$ is the element-wise soft-thresholding operator in Eq. (29).

Algorithm 2. SVM GraphNet classification update using infimal convolution

1. Given a set of data and parameters $\Omega = \{X, y, \lambda_1, \lambda_G\}$, previous coefficient estimates $\hat{\alpha}^{(r)}, \hat{\beta}_0^{(r)}, \hat{\beta}^{(r)}$, and $p \times p$ positive semidefinite constraint graph $G \in S_+^{p \times p}$, let

$$\hat{\gamma}^{(r)} = [\hat{\beta}_0^{(r)} \hat{\beta}^{(r)} \hat{\alpha}^{(r)}]^T$$

$$Z = [y^T [1_{n \times 1} X] \ I_{n \times n}].$$

2. Choose coordinate j using essentially cyclic rule (Tseng, 2001) and fix $\tilde{\gamma} = \{\gamma_k^{(r)} | k \neq j\}$, $\tilde{Z} = Z_{\cdot, \neq j}$, $\tilde{\beta} = \{\beta_k^{(r)} | k \neq j\}$, $\tilde{X} = X_{\cdot, \neq j}$.
3. Update $\hat{\gamma}_j^{(r)}$ using

$$\hat{\gamma}_j^{(r+1)} \leftarrow \begin{cases} \tilde{\gamma}^T \tilde{Z} 1_{n \times 1} + n(\gamma_j - 1) & \text{if } j = 0 \\ \frac{S((\tilde{Z}^T \tilde{\gamma} - 1_{n \times 1}^T X_j - (\lambda_2/2)\tilde{\beta}^T(G'_{\neq j})_j, \lambda_1/2))}{X_j^T X_j + \lambda_G G'_{jj}} & \text{if } j \in \{1, \dots, p\} \\ H((\tilde{Z}\tilde{\gamma})_j - 1, \delta) & \text{if } j \in \{p+1, \dots, p+n\}, \end{cases}$$

where $S(x, \lambda)$ is the element-wise soft-thresholding operator, $H(x, \delta)$ is given in Eq. (31), and G' is the appropriately augmented G given in Eq. (19).

4. Repeat (1)–(3) cyclically for all $j \in \{1, \dots, p+n\}$ until convergence (see discussion of convergence in Friedman et al. (2007a)).
5. Optional: rescale resulting estimates using method from the section “Rescaling coefficients to account for “double shrinking””.

Derivation of updates in Algorithm 2

Following the description of the SVM given in the section “Turning regression methods into classifiers: relating Support Vector Machines (SVM) to penalized regression”, we can take the same approach used to derive the robust GraphNet estimates with the Support Vector GraphNet estimates in the section “Huberized Support Vector Machine (SVM) GraphNet for classifications”, which we can write as

$$\hat{\gamma} = \underset{\gamma}{\operatorname{argmin}} (1/2\delta) \|1_{n \times 1} - Z\gamma\|_2^2 + \lambda_G \gamma_{\neq 0}^T G' \gamma_{\neq 0} + \sum_{j=0}^p w_j |\gamma_j| + \sum_{j=p+1}^{p+n} w_j \max(0, \gamma_j)$$

where $Z = [y^T [1_{n \times 1} X] \ I_{n \times n}]$, $\gamma = [\beta_0 \ \beta \ \alpha]$, $w_j = \begin{cases} 0 & \text{if } j = 0 \\ \lambda_1 & \text{if } j = 1, \dots, p \\ 1 & \text{if } j = p+1, \dots, p+n \end{cases}$

$$G' = \begin{bmatrix} 0 & 0_{1 \times p} & 0_{1 \times n} \\ 0_{p \times 1} & G & 0_{p \times n} \\ 0_{n \times 1} & 0_{n \times 1} & 0_{n \times n} \end{bmatrix} \in S_+^{(p+n+1) \times (p+n+1)}.$$

During coordinate wise descent, only one of the separable penalty functions has an “active” variable per descent step. Letting $h(\gamma_j) = \max(0, \gamma_j)$, we thus have

$$\hat{\gamma}_j = \begin{cases} \underset{\gamma_j}{\operatorname{argmin}} (1/2\delta) \|1_{n \times 1} - \tilde{Z}\tilde{\gamma} - Z_j \gamma_j\|_2^2 & \text{if } j = 0 \\ \underset{\gamma_j}{\operatorname{argmin}} (1/2\delta) \|1_{n \times 1} - \tilde{Z}\tilde{\gamma} - Z_j \gamma_j\|_2^2 + \lambda_G (\tilde{\gamma}^T (G'_{\neq j})_j \gamma_j + G'_{jj} \gamma_j^2) + \lambda_1 |\gamma_j| & \text{if } j \in \{1, \dots, p\} \\ \underset{\gamma_j}{\operatorname{argmin}} (1/2\delta) \|1_{n \times 1} - \tilde{Z}\tilde{\gamma} - Z_j \gamma_j\|_2^2 + h(\gamma_j) & \text{if } j \in \{p+1, \dots, p+n\}. \end{cases}$$

Then since

$$Z_j = \begin{cases} 1_{n \times 1} & \text{if } j = 0 \\ X_j & \text{if } j \in \{1, \dots, p\} \\ e_j & \text{if } j \in \{p+1, \dots, p+n\}, \end{cases}$$

(where e_j is the vector of all zeros except for the j th element, which is 1) we have

$$\hat{\gamma}_j \leftarrow \begin{cases} -1_{n \times 1}^T Z_j + (\tilde{Z}\tilde{\gamma})^T Z_j + \gamma_j Z_j^T Z_j & \text{if } j = 0 \\ \frac{S((\tilde{Z}\tilde{\gamma})^T Z_j - 1_{n \times 1}^T Z_j - (\lambda_G/2)\tilde{\gamma}^T(G'_{\neq j})_j, \lambda_1/2)}{Z_j^T Z_j + \lambda_G G'_{jj}} & \text{if } j \in \{1, \dots, p\} \\ \frac{H((\tilde{Z}\tilde{\gamma})^T e_j - 1_{n \times 1}^T e_j, \delta)}{e_j^T e_j} & \text{if } j \in \{p+1, \dots, p+n\}, \end{cases}$$

yielding update:

$$\hat{\gamma}_j \leftarrow \begin{cases} \tilde{\gamma}^T \tilde{Z} 1_{n \times 1} + n(\gamma_j - 1) & \text{if } j = 0 \\ \frac{S\left(\left(\tilde{Z}^T \tilde{\gamma} - 1_{n \times 1}\right)^T X_{j-} - (\lambda_G/2) \tilde{\beta}^T (G'_{\neq j})_{\cdot j}, \lambda_1/2\right)}{X_{j-}^T X_{j-} + \lambda_G G_{jj}} & \text{if } j \in \{1, \dots, p\} \\ H\left(\left(\tilde{Z} \tilde{\gamma}\right)_j - 1, \delta\right) & \text{if } j \in \{p+1, \dots, p+n\}, \end{cases}$$

where $S(x, \lambda)$ is the element-wise soft-thresholding operator in Eq. (29) and

$$H(x, \delta) = \begin{cases} x - \delta & \text{if } x < 1 \\ x & \text{otherwise.} \end{cases} \quad (31)$$

Parameter grid used in cross-validation

Parameters $\{\lambda_1, G, \lambda_G, \delta, \lambda_1^*\}$ were taken over the following grid of values:

$$\begin{aligned} \lambda_1 &\in \{10, 11, \dots, 99\} \\ G &\in \{L, L + \eta I, L + 10^2 \eta I, L + 10^3 \eta I, L + 10^4 \eta I\} \text{ where } \eta = 1/\lambda_G \text{ for } \lambda_G \\ &> 0 \text{ and } 1 \text{ otherwise} \\ \lambda_G &\in \{0, 10^1, 10^2, 10^3, 10^4, 10^5\} \\ \delta &\in \{0.2, 0.3, 0.4, 0.5, 0.6, 0.7, 1, 2, 10, 100\} \\ \lambda_1^* &\in \{1, 10^{-1}, 10^{-2}\}. \end{aligned}$$

The linear SVM was fit over parameters

$$C \in \{10^{-6}, 10^{-5}, 10^{-4}, 10^{-3}, 10^{-2}, 10^{-1}, 10^{-0}, 2, 3, 4, 5, 6, 7, 10^1, 10^2, 10^3\}. \quad (32)$$

References

- Adler, R.J., Taylor, J.E., 2000. Random Fields and Geometry. Rice University Technical Report No. TR2011-03 (Preprint available on arXiv:1102.3074).
- Barbieri, M., Berger, J., 2004. Optimal predictive model selection. *Ann. Stat.* 32, 870–897.
- Belkin, M., Niyogi, P., 2008. Towards a theoretical foundation for Laplacian-based manifold methods. *J. Comput. Syst. Sci.* 74, 1289–1308.
- Belkin, M., Niyogi, P., Sindhawani, V., 2006. On manifold regularization. *J. Mach. Learn. Res.* 7, 2399–2434.
- Boyd, S., Vandenberghe, L., 2004. Convex Optimization.
- Bray, S., Chang, C., Hoeff, F., 2009. Applications of multivariate pattern classification analyses in developmental neuroimaging of healthy and clinical populations. *Front. Hum. Neurosci.* 3 (32), 1–12.
- Breiman, L., Ihaka, R., 1984. Univ of California at Berkeley Technical Report: Nonlinear Discriminant Analysis via Scaling and ACE.
- Brodersen, K., Haiss, F., Ong, C.S., Jung, F., Tittgemeyer, M., Buhmann, J.M., Weber, B., Stephan, K.E., 2011. Model-based feature construction for multivariate decoding. *NeuroImage* 56 (2), 601–615.
- Candes, E.J., Wakin, M.B., Boyd, S.P., 2003. Optimally sparse representation in general (nonorthogonal) dictionaries via l_1 minimization. *PNAS* 100 (5), 2197–2202.
- Candes, E.J., Wakin, M.B., Boyd, S.P., 2008. Enhancing sparsity by reweighted l_1 minimization. *J. Fourier Anal. Appl.* 14, 69–82.
- Carroll, M., Cecchi, G., Rish, I., Garg, R., Rao, A.R., 2009. Prediction and interpretation of distributed neural activity with sparse models. *NeuroImage* 44 (1), 112–122.
- Chappell, M.A., Groves, A.R., Whitcher, B., Woolrich, M.W., 2009. Variational Bayesian inference for a nonlinear forward model. *IEEE Trans. Signal Proc.* 57 (1), 223–236.
- Clemmensen, L., Hastie, T., Witten, D., Erbsboll, B., 2011. Sparse discriminant analysis. *Technometrics* 53 (4), 406–413.
- Cortes, C., Vapnik, V., 1995. Support-vector networks. *Mach. Learn.* 20 (3), 273–297.
- Cox, R.W., 1996. AFNI: software for analysis and visualization of functional magnetic resonance images. *Comput. Biomed. Res.* 29, 162–173.
- De Martino, F., Gentile, F., Esposito, F., Balsi, M., Di Salle, F., Goebel, R., Formisano, E., 2007. Classification of fMRI independent components using IC-fingerprints and support vector machine classifiers. *NeuroImage* 34, 177–194.
- Donoho, D.L., 1995. De-noising by soft-thresholding. *IEEE Trans. Inf. Theory* 41 (3), 613–627.
- Donoho, D.L., 2006. For most large underdetermined systems of linear equations, the minimal l_1 -norm solution is also the sparsest solution. *Commun. Pure Appl. Math.* 59 (6), 797–829.
- Etzel, J.A., Gazzola, V., Keysers, C., 2009. An introduction to anatomical ROI-based fMRI classification analysis. *Brain Res.* 1282, 114–125.
- Fan, J., Li, R., 2001. Variable selection via nonconcave penalized likelihood and its oracle properties. *J. Am. Stat. Assoc.* 96 (456), 1348–1360.
- Friedman, J.H., 1997. On bias, variance, 0/1-loss, and the curse-of-dimensionality. *Data Min. Knowl. Disc.* 1, 55–77.
- Friedman, J., Hastie, T., Höfling, H., Tibshirani, R., 2007a. Pathwise coordinate optimization. *Ann. Appl. Stat.* 1 (2), 302–332.
- Friedman, J.H., Hastie, T., Höfling, H., Tibshirani, R., 2007b. Pathwise coordinate optimization. *Ann. Appl. Stat.* 1 (2), 302–332.
- Friedman, J., Hastie, T., Tibshirani, R., 2010. Regularization paths for generalized linear models via coordinate descent. *J. Stat. Softw.* 33 (1), 1–22.
- Friston, K., Holmes, A., Worsley, K., Poline, J., 1995. Statistical parametric maps in functional imaging: a general linear approach. *Hum. Brain Mapp.* 2, 189–210.
- Glover, G.H., Law, C.S., 2001. Spiral in/out BOLD FMRI for increased SNR and reduced susceptibility artifacts. *Magn. Reson. Med.* 46, 512–522.
- Groseknick, L., Greer, S.M., Knutson, B., 2008. Interpretable classifiers for FMRI improve prediction of purchases. *IEEE Trans. Neural Syst. Rehabil. Eng.* 16 (6), 539–548.
- Groseknick, L., Anderson, T., Smith, S.J., 2009a. Elastic source selection for in vivo imaging of neuronal ensembles. *Biomedical Imaging: From Nano to Macro*, 6th IEEE International Symposium on.
- Groseknick, L., Klingenberg, B., Greer, S., Taylor, J.E., Knutson, B., 2009b. Whole-brain sparse penalized discriminant analysis for predicting choice. *NeuroImage (Supplement 1)*, S58.
- Guyon, I., Weston, J., Barnhill, S., Vapnik, V., 2002. Gene selection for cancer classification using support vector machines. *Mach. Learn.* 46, 389–422.
- Hanke, M., Halchenko, Y., Sederberg, P., 2009. PyMVPA: a Python toolbox for multivariate pattern analysis of fMRI data. *Neuroinformatics* 7 (1), 37–53.
- Hare, T.A., O'Doherty, J., Camerer, C.F., Schultz, W., Rangel, A., 2008. Dissociating the role of the orbitofrontal cortex and the striatum in the computation of goal values and prediction errors. *J. Neurosci.* 28 (22), 5623–5630.
- Hastie, T., Tibshirani, R., Buja, A., 1994. Flexible Discriminant Analysis by Optimal Scoring. *J. Am. Stat. Assoc.* 89 (428), 1255–1270.
- Hastie, T., Buja, A., Tibshirani, R., 1995. Penalized Discriminant Analysis. *Ann. Stat.* 23 (1), 73–102.
- Hastie, T., Tibshirani, R., Friedman, J., 2009. The Elements of Statistical Learning: Data Mining, Inference, and Prediction.
- Haynes, J., Rees, G., 2006. Decoding mental states from brain activity in humans. *Nat. Rev. Neurosci.* 7, 523–534.
- Haynes, J., Sakai, K., Rees, G., Gilbert, S., 2007. Reading hidden intentions in the human brain. *Curr. Biol.* 17 (4), 323–328.
- Hoerl, A.E., Kennard, R.W., 1970. Ridge regression: applications to nonorthogonal problems. *Technometrics* 12 (1), 69–82.
- Huber, P.J., Ronchetti, E.M., 2009. Robust Statistics.
- Hutchinson, R.A., Niculescu, R.S., Keller, T.A., Rustandi, I., Mitchell, T.M., 2009. Modeling fMRI data generated by overlapping cognitive processes with unknown onsets using Hidden Process Models. *NeuroImage* 46 (1), 87–104.
- Jenatton, R., Audibert, J.-Y., Bach, F., 2011. Structured variable selection with sparsity-inducing norms. *J. Mach. Learn. Res.* 12, 2777–2824.
- Jimenez, A.B., Lazaro, J.L., Dorronsoro, J.R., 2009. Finding optimal model parameters by deterministic and annealed focused grid search. *Neurocomputing* 72 (13–15), 2824–2832.
- Karmarkar, U.R., Shiv, B., Knutson, B., submitted for publication. Sticker shock: the neural and behavioral impact of price primacy on purchasing.
- Knutson, B., Greer, S.M., 2008. Anticipatory affect: neural correlates and consequences for choice. *Philos. Trans. R. Soc. Lond. B Biol. Sci.* 363 (1511), 3771–3786.
- Knutson, B., Adams, C.M., Fong, G.W., Hommer, D., 2001. Anticipation of increasing monetary reward selectively recruits nucleus accumbens. *J. Neurosci.* 21 (16), 1–5.
- Knutson, B., Taylor, J., Kaufman, M., Peterson, R., Glover, G., 2005. Distributed neural representation of expected value. *J. Neurosci.* 25, 4806–4812.
- Knutson, B., Rick, S., Wimmer, G.E., Prelec, D., Loewenstein, G., 2007. Neural predictors of purchases. *Neuron* 53, 147–156.
- Lehmann, E.L., Casella, G., 1998. Theory of Point Estimation.
- Leng, C., 2008. Sparse optimal scoring for multiclass cancer diagnosis and biomarker detection using microarray data. *Comput. Biol. Chem.* 32, 417–425.
- Li, C., Li, H., 2008. Network-constrained regularization and variable selection for analysis of genomic data. *Bioinformatics* 24 (9), 1175–1182.
- Li, Y., Namburi, P., Yu, Z., Guan, C., Feng, J., Gu, Z., 2009. Voxel selection in fMRI data analysis based on a sparse representation. *IEEE Trans. Biomed. Eng.* 56 (10), 2439–2451.
- McCoy, A.N., Crowley, J.C., Haghighian, G., Dean, H.L., Platt, M.L., 2003. Saccade reward signals in posterior cingulate cortex. *Philos. Trans. R. Soc. Lond. B Biol. Sci.* 40 (5), 1031–1040.
- Meinshausen, N., Bühlmann, P., 2010. Stability Selection. *J. R. Stat. Soc. Ser. B* 72 (4), 417–473.
- Merchante, L.F.S., Grandvalet, Y., Govaert, G., 2012. An efficient approach to sparse linear discriminant analysis. *Proceedings of the International Conference on Machine Learning (ICML)*.
- Michel, V., Gramfort, A., Varoquaux, G., Eger, E., Thirion, B., 2011. Total variation regularization for fMRI-based prediction of behavior. *IEEE Trans. Med. Imaging* 30 (7), 1328–1340.
- Mitchell, T.M., Hutchinson, R., Niculescu, R., 2004. Learning to decode cognitive states from brain images. *Mach. Learn.* 57 (1–2), 145–175.

- Mohamed, S., Heller, K., Ghahramani, Z., 2011. Bayesian and L1 Approaches to Sparse Unsupervised Learning (arXiv:1106.1157v2).
- Mourão-Miranda, J., Friston, K., Brammer, M., 2007. Dynamic discrimination analysis: a spatial-temporal SVM. *NeuroImage* 36, 88–99.
- Ng, B., Silless, V., Varoquaux, G., Yoline, J.-B., Thirion, B., Abugharbieh, R., 2012. Connectivity-informed sparse classifiers for fMRI brain decoding. *Pattern Recognition in NeuroImaging (PRNI), IEEE 2012 International Workshop on*, pp. 101–104.
- Norman, K., Polyn, S., Detre, G., Haxby, J., 2006. Beyond mind-reading: multi-voxel pattern analysis of fMRI data. *Trends Cogn. Sci.* 10 (9), 424–430.
- O'Toole, A., Jiang, F., Abdi, H., Penard, N., 2007. Theoretical, statistical, and practical perspectives on pattern-based classification. *J. Cogn. Neurosci.* 2007 (19), 1735–1752.
- Peelen, M., Fei-Fei, L., Kastner, S., 2009. Neural mechanisms of rapid natural scene categorization in human visual cortex. *Nature* 460, 94–97.
- Pereira, F., Mitchell, T.M., Botvinick, M., 2009. Machine learning classifiers and fMRI: a tutorial overview. *NeuroImage* 45 (1), S199–S209 (Supplement).
- Polyn, S., Natu, V., Cohen, J., Norman, K., 2005. Category-specific cortical activity precedes retrieval during memory search. *Science* 310 (5756), 1963–1966.
- Ravikumar, P., Vu, V.Q., Yu, B., Naselaris, T., Kay, K.N., Gallant, J.L., 2009. Nonparametric sparse hierarchical models describe V1 fMRI responses to natural images: Advances in Neural Information Processing Systems, 21.
- Rockafellar, T.J., 1970. *Convex Analysis*.
- Rudin, L.I., Osher, S., Fatemi, E., 1992. Nonlinear total variation based noise removal algorithms. *Physica D* 50, 259–268.
- Ryali, S., Supekar, K., Abrams, D.A., Menon, V., 2010. Sparse logistic regression for whole-brain classification of fMRI data. *NeuroImage* 51 (2), 752–764.
- Shinkareva, S.V., Mason, R.A., Malave, V.L., Wang, W., Mitchell, T.M., Just, M.A., 2008. Using fMRI brain activation to identify cognitive states associated with perception of tools and dwellings. *PLoS One* 3 (1).
- Slawski, M., zu Castell, W., Tutz, G., 2010. Feature selection guided by structural information. *Ann. Appl. Stat.* 4 (2), 1055–1080.
- Stein, C., 1956. Inadmissibility of the usual estimator for the mean of a multivariate normal distribution. *Proc. Third Berkeley Symp. on Math. Statist. and Prob.*, vol. 1, pp. 197–206.
- Tibshirani, R., 1996. Regression shrinkage and selection via the lasso. *J. R. Stat. Soc. Ser. B* 58 (1), 267–288.
- Tibshirani, R., Taylor, J.E., 2011. The solution path of the generalized lasso. *Ann. Stat.* 3, 1335–1371.
- Tibshirani, R., Saunders, M., Rosset, S., Zhu, J., Knight, K., 2005. Sparsity and smoothness via the fused lasso. *J. R. Stat. Soc. Ser. B* 67 (1), 91–108.
- Tibshirani, R., Bien, J., Friedman, J., Hastie, T., Simon, N., Taylor, J.E., Tibshirani, R.J., 2012. Strong rules for discarding predictors in lasso-type problems. *J. R. Stat. Soc. Ser. B* 74 (2), 245–266.
- Tikhonov, A., 1943. On the Stability of Inverse Problems.
- Tseng, P., 1988. Technical Report LIDS-P, 1840. Massachusetts Institute of Technology, Laboratory for Information and Decision Systems (arXiv:0903.2515).
- Tseng, P., 2001. Convergence of block coordinate descent method for nondifferentiable maximization. *J. Optim. Theory Appl.* 109, 474–494.
- van der Kooij, A.J., 2007. Prediction accuracy and stability of regression with optimal scaling transformations. Technical Report, Dept. Data Theory, Leiden Univ.
- van Gerven, M.A.J., Heskes, T., 2012. A linear Gaussian framework for decoding of perceived images. *International Workshop on Pattern Recognition in NeuroImaging (PRNI), IEEE 2012*, pp. 1–4.
- van Gerven, M.A.J., Cseke, B., de Lange, F.P., Heskes, T., 2010. Efficient Bayesian multivariate fMRI analysis using a sparsifying spatio-temporal prior. *NeuroImage* 150–161.
- Wager, T.D., Atlas, L.Y., Leotti, L.A., Rillings, J.K., 2011. Predicting individual differences in placebo analgesia: contributions of brain activity during anticipation and pain experience. *J. Neurosci.* 31 (2), 439–452.
- Wang, L., Zhu, J., Zou, H., 2008a. Hybrid Huberized Support Vector Machines for microarray classification and gene selection. *Bioinformatics* 24 (3), 412–419.
- Wang, Y., Junfeng, Y., Yin, W., Zhang, Y., 2008b. A new alternating minimization algorithm for Total Variation image reconstruction. *SIAM J. Imaging Sci.* 1 (3), 248–272.
- Wipf, D., Nagarajan, S., 2008. A new view of automatic relevance determination: Advances in Neural Information Processing Systems, 20.
- Witten, D.M., Tibshirani, R., 2011. Penalized classification using Fisher's linear discriminant. *J. R. Stat. Soc. Ser. B* 73 (5), 753–772.
- Worsley, K.J., Taylor, J.E., Tomaiuolo, F., Lerch, J., 2004. Unified univariate and multivariate random field theory. *NeuroImage* 23, S189–S195.
- Yamashita, O., Sato, M., Yoshioka, T., Tong, F., Kamitani, Y., 2008. Sparse estimation automatically selects voxels relevant for the decoding of fMRI activity patterns. *NeuroImage* 42 (4), 1414–1429.
- Zhou, S., van de Geer, S., Bühlmann, P., 2011. Adaptive lasso for high dimensional regression and Gaussian graphical modeling. *Electron. J. Stat.* 5, 688–749.
- Zou, H., 2006. The adaptive lasso and its oracle properties. *J. Am. Stat. Assoc.* 101 (467), 1418–1429.
- Zou, H., Hastie, T., 2005. Regularization and variable selection via the elastic net. *J. R. Stat. Soc. Ser. B* 67 (2), 301–320.
- Zou, H., Zhang, H., 2009. On the adaptive elastic-net with a diverging number of parameters. *Ann. Stat.* 37 (4), 1733–1751.
- Zou, H., Hastie, T., Tibshirani, R., 2007. On the “degrees of freedom” of the lasso. *Ann. Stat.* 35 (5), 2173–2192.